Contrast-Dependent Nonlinearities Arise Locally in a Model of Contrast-Invariant Orientation Tuning

ANDREW KAYSER,[1,3,4]* NICHOLAS J. PRIEBE,[1,3,4]* AND KENNETH D. MILLER[1–5]
[1]*Department of Physiology,* [2]*Department of Otolaryngology,* [3]*Neuroscience Graduate Program,* [4]*W. M. Keck Center for Integrative Neuroscience, and* [5]*Sloan Center for Theoretical Neurobiology, University of California, San Francisco, California 94143-0444*

Received 5 July 2000; accepted in final form 17 January 2001

Kayser, Andrew, Nicholas J. Priebe, and Kenneth D. Miller. Contrast-dependent nonlinearities arise locally in a model of contrast-invariant orientation tuning. *J Neurophysiol* 85: 2130–2149, 2001. We study a recently proposed "correlation-based," push-pull model of the circuitry of layer 4 of cat visual cortex. This model was previously shown to explain the contrast-invariance of cortical orientation tuning. Here we show that it can simultaneously account for several contrast-dependent (c-d) "nonlinearities" in cortical responses. These include an advance with increasing contrast in the temporal phase of response to a sinusoidally modulated stimulus; a change in shape of the temporal frequency tuning curve, so that higher temporal frequencies may give little or no response at low contrast but reasonable responses at high contrast; and contrast saturation that occurs at lower contrasts in cortex than in the lateral geniculate nucleus (LGN). In the context of the model circuit, these properties arise from a mixture of nonlinear cellular and synaptic mechanisms: short-term synaptic depression, spike-rate adaptation, contrast-induced changes in cellular conductance, and the nonzero spike threshold. The former three mechanisms are sufficient to explain the experimentally observed increase in c-d phase advance in cortex relative to LGN. The c-d changes in temporal frequency tuning arise as a threshold effect: voltage modulations in response to higher-frequency inputs are only slightly above threshold at lower contrast, but become robustly suprathreshold at higher contrast. The other three nonlinear mechanisms also play a crucial role in this result, allowing contrast dependence of temporal frequency tuning to coexist with contrast-invariance of orientation tuning. Contrast saturation, and the observation that responses to stimuli of increasing temporal frequency saturate at increasingly high contrasts, can be induced both by the model's push-pull inhibition and by synaptic depression. Previous proposals explained these nonlinear response properties by assuming contrast-invariant orientation tuning as a starting point, and adding normalization by shunting inhibition derived equally from cells of all preferred orientations. The present proposal simultaneously explains both contrast-invariant orientation tuning and these contrast-dependent nonlinearities and requires only processing that is local in orientation, in agreement with intracellular measurements.

INTRODUCTION

The response properties of simple cells in layer 4 of cat primary visual cortex (V1) serve as a model system for studying the mechanisms underlying cerebral cortical processing. These cells are perhaps the best-studied cortical cells and are the site of emergence of the strong selectivity for stimulus orientation seen throughout visual cortex (Hubel and Wiesel 1962).

One of the defining characteristics of simple cells is the largely linear nature of their responses. Their responses to arbitrary stimuli can be reasonably well predicted from a weighted sum of stimulus intensity, where the weighting is given by the cell's receptive field and negative values of the weighted sum are taken to yield zero response (DeAngelis et al. 1993; Hubel and Wiesel 1962; Jones and Palmer 1987). As predicted by a linear response model, the shape of a simple cell's orientation tuning curve is invariant to changes in stimulus contrast (Sclar and Freeman 1982; Skottun et al. 1987): a change in contrast scales all responses by a constant, rather than changing the form of the response tuning curve.

However, other aspects of simple cell responses show a nonlinear dependence on stimulus contrast (reviewed in Carandini et al. 1998). In this paper we will examine three such properties: *1*) contrast-dependent phase advance: as the contrast of a sinusoidal grating stimulus increases, the response of a cortical cell occurs earlier in the stimulus cycle (Albrecht 1995; Dean and Tolhurst 1986); *2*) contrast-dependent temporal frequency tuning: higher temporal frequencies that yield small or zero responses at low contrast yield reasonable responses at high contrast (Albrecht 1995; Holub and Morton-Gibson 1981); and *3*) contrast saturation: the change in response amplitude with contrast has a sigmoidal rather than linear dependence on contrast, saturating at intermediate contrasts (e.g., Albrecht 1995). The third property involves the nonlinear dependence of scaling on contrast. The first two involve changes in response more complex than a simple scaling by contrast: responses either move earlier in time (property 1) or increase differentially across the tuning curve (property 2).

In this paper, we address the question of how a single model circuit, consistent with existing experimental knowledge of cat visual cortex, can simultaneously account for both the linear-like response scaling of contrast-invariant orientation tuning and the above three nonlinear response properties. In principle, accounting for nonlinear response properties in isolation may

* A. Kayser and N. J. Priebe contributed equally to the modeling in this paper.

Address for reprint requests: K. D. Miller, Dept. of Physiology, UCSF, 513 Parnassus, San Francisco, CA 94143-0444 (E-mail: ken@phy.ucsf.edu).

The costs of publication of this article were defrayed in part by the payment of page charges. The article must therefore be hereby marked "*advertisement*" in accordance with 18 U.S.C. Section 1734 solely to indicate this fact.

not be difficult, given the many inherently nonlinear properties of the synapses, cells, and circuits involved. We suggest that the true difficulty lies in simultaneously accounting for both linear-like and nonlinear response properties: how can the underlying nonlinear mechanisms be manifest in some aspects of response and yet simultaneously be hidden in other aspects? Indeed, the difficulty of generating any linear-like responses at all is well illustrated by the contrast-invariance of orientation tuning in response to drifting sinusoidal luminance gratings. LGN cells do not provide linear input to simple cells, because their response rates cannot decrease below zero. As a result, LGN mean firing rates increase with contrast. Under a linear response model, an increase in stimulus contrast would increase the amplitude of temporal modulation of firing rates without affecting mean rates. Furthermore, cortical cells integrate this input through the nonlinearity of a nonzero spike threshold. Due to the increase both in modulations and means of LGN firing rates, a broader range of stimulus orientations should produce suprathreshold LGN input at higher contrasts. Thus the orientation tuning of the LGN input to a simple cell should widen with increasing stimulus contrast.

We have recently demonstrated (Troyer et al. 1998) that the contrast-invariance of orientation tuning can be accounted for by the combination of *1*) a simple model intracortical circuit motivated by numerous intracellular studies (e.g., Anderson et al. 2000; Chung and Ferster 1998; Ferster 1986, 1988; Ferster et al. 1996; Hirsch et al. 1998; Nelson et al. 1994) and *2*) a "Hubel-Wiesel" (1962) arrangement of lateral geniculate nucleus (LGN) inputs to simple cells, in which oriented bands of ON- or OFF-center LGN inputs provide input to the ON- or OFF-subregions, respectively, of the simple cell's receptive field. Here we demonstrate, for the first time, a unified mechanistic account of both the linear and nonlinear aspects of simple cell responses. Our previous model incorporated a number of nonlinear mechanisms, including spike-rate adaptation, contrast-induced changes in cellular conductance, and the nonzero spike threshold. We now add one additional nonlinear mechanism, short-term synaptic depression (Abbott et al. 1997; Tsodyks and Markram 1997). We show that the resulting model explains the three nonlinear properties noted above, while retaining contrast-invariant orientation tuning.

Importantly, this is the first explanation of these properties using a model circuit that is purely local in orientation (see DISCUSSION for other models). That is, both the excitatory and the inhibitory intracortical input received by a simple cell comes primarily from cells having similar preferred orientation, as suggested by numerous experiments in cat V1 (Anderson et al. 2000; Chung and Ferster 1998; Ferster 1986, 1988; Ferster et al. 1996; Hirsch et al. 1998).

Some of these results have appeared in abstract form (Priebe et al. 1997).

MODELING FRAMEWORK

We begin by summarizing the essential information about our model needed to understand our results. Full details sufficient to replicate our work are in APPENDIX A.

Intracortical circuit

We study a circuit (Troyer et al. 1998) in which *1*) geniculocortical synaptic weights to a cell are described by Gabor functions (Jones and Palmer 1987), with ON-center (OFF-center) inputs corresponding to positive (negative) portions of the Gabor; and *2*) intracortical connections are made between cortical cells based on the correlations between their receptive fields (RFs), i.e., between the geniculocortical synaptic weights they receive. An excitatory cell makes strong connections onto other excitatory cells with which it is strongly correlated; an inhibitory cell makes strong connections onto excitatory cells with which it is strongly anticorrelated. The dominant resulting connections follow a "push-pull" scheme and are illustrated in Fig. 1. A crucial requirement is that inhibition be dominant: the feed-forward inhibitory pathway LGN $\rightarrow$ I $\rightarrow$ E must have stronger overall gain than the feed-forward excitatory pathway LGN $\rightarrow$ E (where E and I indicate excitatory and inhibitory cortical cells, respectively), as assessed by the mean feed-forward inhibition exceeding mean feed-forward excitation over a cycle of response to a sinusoidal stimulus. More specifically, the mean conductance opened by the two pathways over a cycle must have a sufficiently subthreshold reversal

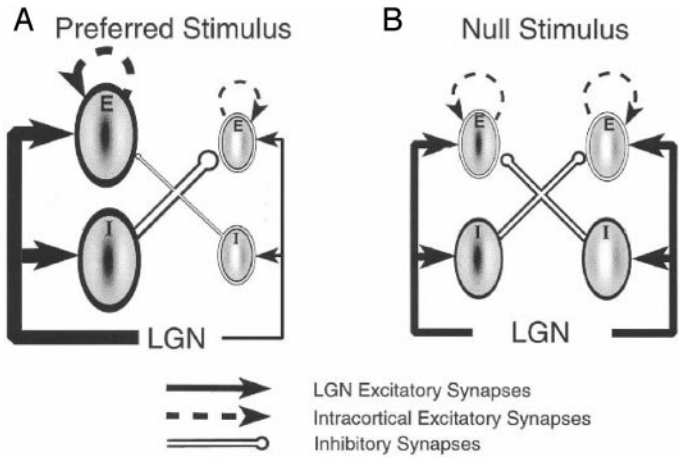

FIG. 1. Cartoon of the cortical circuit studied. All neurons receive excitatory geniculocortical connections from the lateral geniculate nucleus (LGN) as determined by Gabor functions (illustrated by modulations on a gray/uniform background): ON inputs at a given retinal location within the receptive field (RF) are represented by white; OFF inputs by black. All illustrated RFs are centered at a common retinotopic position. Neurons with RFs of similar preferred orientation but opposite spatial phase are connected by inhibitory synaptic weights (white, with black outline), while neurons with similar preferred orientations and similar spatial phases are connected by excitatory synaptic weights (black arrows). *A*: response to a full-field sinusoidal grating of the preferred orientation. When the stimulus maximally overlaps the RFs on the left, the geniculocortical input to those cells is maximal (large solid black arrows), while the input to the RFs of opposite spatial phase (those on the *right* of *A*) is minimal (small solid black arrows). Neurons of the well-stimulated phase will fire robustly, and the strongly activated inhibitory cells send inhibition only to the weakly stimulated anti-phase excitatory neurons, which do not fire. As a result, as the grating moves across the neurons' RFs, the excitatory cortical neurons will produce a strongly time-varying response at the same temporal frequency as that of the input. *B*: response to a full-field sinusoidal grating of the null orientation (orthogonal to the preferred). Because LGN cells respond to all orientations, the geniculocortical input is still present, but the input to each phase is approximately equal. Inhibition is equally strong from neurons of each phase to their anti-phase excitatory-cell partners. Since inhibition is dominant, none of the excitatory cells fire. The actual circuit studied included cells of many preferred orientations and spatial phases and, for the spiking model, many retinotopic positions. Connections were based on correlations between RFs. Cartoon illustrates dominant connections; resulting circuit behavior can be well understood from this simplified version of the circuit (Troyer et al. 1998).

potential to prevent spiking to a stimulus with orientation orthogonal to a cell's preferred orientation.

This architecture can account for cortical orientation tuning and its contrast invariance (Troyer et al. 1998). How does this circuitry account for orientation tuning? For a stimulus at a cell's preferred orientation and spatial phase, other neurons with similar preferred orientation and spatial phase (both excitatory and inhibitory) are strongly activated. However, the inhibition is directed onto cells with similar preferred orientation but antiphase (opposite spatial phase) RFs. In the case of a drifting sinusoidal grating of the preferred orientation, the resulting inhibition received by a cell comes out-of-phase with its excitation, permitting excitatory cells to respond during the temporal phase in which more excitation is received than inhibition (Fig. 1*A*). As the orientation is shifted away from the preferred, temporal modulation of both feed-forward excitation and feed-forward inhibition decreases. Since inhibition is dominant in the mean, at some orientation the modulation is small enough that inhibition is dominant at all times, and the cell cannot fire. In particular, for a stimulus at a cell's null orientation (perpendicular to the preferred), there is essentially no modulation, inhibitory neurons of both the cell's preferred phase and the opposite phase are continuously activated, and thus excitatory cells of both phases are continuously inhibited (Fig. 1*B*).

The contrast-invariance of orientation tuning arises because an increase in contrast equally increases the geniculocortical drive to a given cell and to the anti-phase cells from which it receives inhibition. Thus the cutoff orientation (the orientation for which input modulation is sufficiently small that inhibition dominates throughout the cycle) remains essentially invariant across contrast. A more detailed analysis is given in Troyer et al. (1998).

Rate model

We studied two forms of model: a conceptual rate model and a more biophysically accurate spiking model. The rate model allowed exploration of the cortical circuit and its elements within a simple framework. This allowed us both to work out the basic mechanisms underlying circuit properties, and to explore a significant portion of the given parameter space, thereby establishing the robustness of these insights. The spiking model, on the other hand, allowed us to establish that the insights gained from the rate model translated to a more detailed, more biophysically realistic setting, and thus provided a verification of the rate model findings. The spiking model also allowed us to examine the role of spike-rate adaptation, which was not easily accommodated in the rate model.

The rate model consisted of 96 excitatory and 96 inhibitory neurons, with RFs of 12 different orientations and 8 different spatial phases, all centered at the same retinotopic point. Connections between cortical neurons were made deterministically based on the correlation between their RFs, as described above. Model neuron firing rates were calculated as the weighted sum of all the input firing rates from geniculocortical, intracortical excitatory, and intracortical inhibitory sources, rectified at a threshold; hence the term, "rate model." The model was described by eight parameters: the thresholds and membrane time constants of excitatory and inhibitory cells, the gains of geniculocortical (G), intracortical inhibitory-to-excitatory (I), and excitatory-to-excitatory (E) cell connections, and a lower bound on the membrane voltage. Appropriate values for these eight variables were obtained by constraining the output of the circuit to match a set of experimental findings, including the width and contrast-invariance of orientation tuning (see APPENDIX A); this set did not include the nonlinear responses properties studied here. In addition, two parameters describe synaptic depression, as described below. For each choice of synaptic depression parameters, we typically show average results over *all* sets of the other parameters that met these criteria, thus examining the robustness of the results across experimentally reasonable model parameters that are consistent with contrast-invariant tuning.

Spiking model

To expand on the insights obtained from the rate model in a more biophysically realistic framework, we used the spiking model of Troyer et al. (1998). One thousand six hundred excitatory and 400 inhibitory neurons were laid out in a ⅔ mm × ⅔ mm cortical grid, with retinotopic position constrained to move smoothly across the grid, and with orientations determined by an experimentally measured map from cat V1. The spatial phase of each RF (which determines the location of its ON and OFF subregions) was chosen randomly. Connections between cortical cells were then made probabilistically based on the correlation between the RFs. All neurons were conductance-based integrate-and-fire cells, matched to data from McCormick et al. (1985) as explained in Troyer and Miller (1997a,b). Excitatory neurons had spike-rate adaptation currents. We included only fast [α-amino-3-hydroxy-5-methyl-4-isoxazolepropionic acid (AMPA) and GABA-A] synaptic currents, deferring examination of slow currents [e.g., *N*-methyl-D-aspartate (NMDA) and GABA-B] to future work (e.g., Krukowski 2000). Again, parameters were chosen to achieve appropriately narrow, contrast-invariant orientation tuning, and nonlinear response properties were then studied (see APPENDIX A). Due to the complexity of the model, we present results for only a single set of circuit parameters for each set of synaptic depression parameters used.

Visual stimuli and LGN inputs

Visual inputs to the models were drifting full-field sinusoidal gratings. LGN responses were assumed to arise from a spike rate that was the sum of a linear stimulus-induced temporal modulation and a constant background rate, with rates rectified at zero. Amplitudes of the stimulus modulation were matched to LGN data on X-cell responses across contrast and temporal and spatial frequency (Sclar 1987), as described in APPENDIX A. The rate model used this rate directly as the LGN response, while the spiking model used Poisson spike trains sampled from these rates.

The geniculocortical synaptic weights to the simple cells in the model layer 4 were described by Gabor functions, with parameters matched to experimental measurements of simple cell RFs. In the rate model, the geniculocortical (G) weights were defined deterministically by the Gabor distribution, with negative Gabor values indicating OFF weights; the spiking model RFs were established probabilistically by sampling from the Gabor distribution.

Synaptic depression

Synaptic depression is a use-dependent decrease in synaptic efficacy (Abbott et al. 1997; Markram and Tsodyks 1996); as the firing rate of a presynaptic neuron increases, the influence of single synapses from that cell onto the postsynaptic neuron declines. Intuitively, this relationship holds because higher firing frequencies prevent recovery from depression between input spikes, as discussed below.

One can characterize synaptic depression by two parameters: f, the ratio of the synaptic efficacy immediately after a presynaptic spike to the efficacy before the spike ($0 \leq f \leq 1$), and τ, the time constant of recovery from depression. Smaller values for f lead to a greater loss of synaptic efficacy after every spike; smaller values of τ cause faster recovery from this depression. In both the rate and spiking models, like forms of depression are used: the rate-model depression equation is equal to the average, over Poisson-sampled spike trains, of the spiking-model depression equation (see APPENDIX B), and their behavior in simulations is qualitatively and quantitatively quite similar.

In the experimental literature, two classes of data appear to be present: one in which synaptic depression is studied through the use of paired-pulse stimuli, and one in which depression is characterized by probing with trains of stimuli (S. Nelson, personal communication). These two types of experiment result in different measured values for f and τ, which we call the "pulse" and "train" parameters, respectively (Table 1). Given this experimental uncertainty in parameter values, we examined all results under both choices of parameters.

Contrast-invariance of orientation tuning

As we have mentioned, one of the criteria for selection of our model parameters was that the resulting circuit should have contrast-invariant orientation tuning. More generally, we have found that the principles outlined in Troyer et al. (1998) suffice to robustly produce contrast-invariant tuning across temporal frequencies and in the presence of synaptic depression, two issues not addressed in the previous work, although we do not discuss this point further here.

EXPERIMENTAL FINDINGS ADDRESSED

Having summarized the model circuit, we now summarize the experimental data on response nonlinearities that we will address with this model.

Contrast-dependent phase advance

Simple cells respond earlier in time to drifting gratings as the contrast of those gratings increases, as quantified by the difference in the phase of the first harmonic (F1) of the cortical spiking responses at each contrast (Albrecht 1995; Dean and Tolhurst 1986). We reviewed the literature to determine the size of this contrast-dependent (c-d) phase advance (Fig. 2). We examined both V1 and LGN c-d phase advance, because only the difference between these values needs to be accounted for by cortical mechanisms. In all cases we report the advance over three octaves of contrast (e.g., the relative advance between 10 and 80% contrast).

For V1 simple cells in the cat, c-d phase advance has been measured for approximately 30 cells (Dean and Tolhurst 1986) in one study, and for over 100 cells in another (Albrecht 1995). Mean c-d phase advances were comparable: 42° for a 2-Hz grating in the former study, 47 and 49° for 2- and 8-Hz gratings, respectively, in the latter. In the LGN, X cells show 25° mean c-d phase advance in response to 8-Hz (Sclar 1987) and 3-Hz (Saul and Humphrey 1990) gratings, while Y cells demonstrate as much or more c-d phase advance as cortical simple cells. Both the LGN and cortical measurements are characterized by large standard deviations. Without a knowledge of the X or Y nature of the geniculocortical inputs to the cortical cells studied previously, it is difficult to know how much c-d phase advance the cortex must add, or even whether it adds any at all. An additional uncertainty is raised by the fact that we are modeling layer 4, where the first transformation of LGN inputs occurs. Further cortical transformations could add more c-d phase advance, so layer 4 might show less c-d phase advance than the cortical mean; however, the data on cortical cells were not broken down by layers.

We make perhaps the simplest assumption: cortical layer 4 should account for the mean difference in c-d phase advance between X cells and V1 simple cells. This is based in part on observations suggesting that X cells are the physiologically dominant input in V1 (Ferster 1990a,b; Ferster and Jagadeesh 1991). Thus we assume that layer 4 must account for roughly 20° of c-d phase advance over 3 octaves of contrast. Note that we do not include LGN c-d phase advance in our simulations, so the simulations should be compared only to this difference between experimentally observed LGN and V1 c-d phase advance.

TABLE 1. *Depression parameters*

	Paired-Pulse Data			Train Data		
Location	f	τ, ms	Layer(s)	f	τ, ms	Layer(s)
G	0.563[a]	99[a]	LGN → IV	0.465[d]	371[d]	LGN → III
E	0.875[b]	57[b]	IV → IV	0.8[e]	472[e]	II/III → II/III
I	0.8[c]	179[c]	IV → IV	0.95[e]	1017[e]	II/III → II/III

Parameters were derived by least-squares fits to data in the figures indicated, except that parameters from the random stimulus train experiments of Song et al. (1999) were taken directly as reported. Geniculocortical data divided readily into pulse (Stratford et al. 1996) and train (Gil et al. 1997) parameter sets. The corresponding intracortical data were then chosen, in the case of the pulse data, from work from the same laboratory (Tarczy-Hornoch 1996; Tarczy-Hornoch et al. 1998); and in the case of the train data, from other work in the rodent that recorded both E and I depression curves (Song et al. 1999). Note also that many of the f and τ values in this table do not describe connections within layer IV, the cortical layer we model in this paper. Where possible, when compiling this table we selected values determined *1*) in layer IV *2*) within primary visual cortex *3*) in the cat. LGN, lateral geniculate nucleus. [a] Stratford et al. (1996, Fig. 1*g*); cat primary visual cortex. [b] Tarczy-Hornoch (1996, Fig. 4.5); cat primary visual cortex. [c] Tarczy-Hornoch et al. (1998, Fig. 4; 0.2-Hz curve); cat primary visual cortex. [d] Gil et al. (1997, Fig. 3); mouse and rat somatosensory cortex. [e] Song et al. (1999); rat primary visual cortex. Note that the τ value from the figure legend in Gil et al. (1997) refers to their exponential fit, *not* to the time constant of a fit to a synaptic depression description.

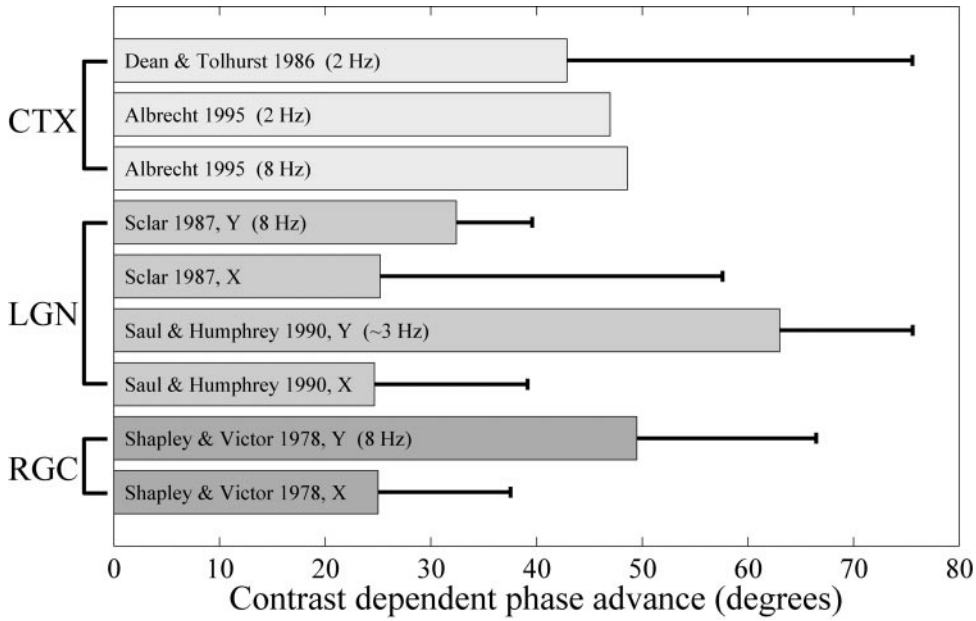

FIG. 2. Experimentally determined values for contrast-dependent (c-d) phase advance in 3 parts of the visual pathway: retinal ganglion cells (RGC, *bottom,* in dark gray), lateral geniculate nucleus (LGN, *middle,* in gray), and striate cortex (CTX, *top,* in light gray). All studies are in cats. c-d phase advance is quantified here as the relative phase difference between responses to stimuli differing by 3 octaves of contrast. The contrasts below are Michelson contrasts $[(I_{max} - I_{min})/(2 * I_{mean})]$. Data represented are mean c-d phase advance (and SD where provided) across cells studied, and are as follows: *1*) Dean and Tolhurst (1986): responses to 5 and 25% contrast drifting gratings for 29 V1 simple cells. We linearly extrapolated, from 2.3 octaves of contrast to 3, the reported mean and SD of c-d phase advance. *2*) Albrecht (1995) (taken from DISCUSSION of that paper): 2 Hz: responses to 5 and 25% contrast drifting gratings, results linearly extrapolated from 2.3 to 3 octaves. 8 Hz: responses to drifting gratings at 10 and 80% contrast (note, c-d phase advance at 8 Hz between 3.5 and 28.3% contrast, also 3 octaves, was 33% larger). All data for V1 simple cells; SDs and number of cells were not reported. *3*) Sclar (1987): mean and SD responses to 10 and 80% contrast drifting gratings for 27 X and 51 Y cells. *4*) Saul and Humphrey (1990): responses to drifting gratings of optimal temporal frequencies for 19 nonlagged X and 8 nonlagged Y cells over a range of contrasts (0.0025–96%). Their linear fits to phases of suprathreshold responses provided slopes with accompanying SDs (both in cycles of phase per octave of contrast), which we multiplied by 3 (converted to degrees) to obtain changes over 3 octaves. *5*) Shapley and Victor (1978): 3.5 and 28.3% contrast (2.5 and 20% RMS contrast) for 8 X and 18 Y cells. Responses to counterphase gratings including 6–8 different temporal frequencies with total contrast as indicated; phase advance of 8-Hz component was determined. In those papers in which phase advance was determined for both X and Y cells, the same temporal frequency was used for each data set; in the figure, this frequency is indicated in the "Y-cell" bar only. We were guided through this data by the lucid discussion of Albrecht (1995).

Contrast-dependent changes in temporal frequency tuning

In response to an increase in stimulus contrast, cortical temporal-frequency tuning curves change their shape. Higher temporal-frequency stimuli that yield small or zero responses at low contrast yield reasonable responses at higher contrast. One measure of this is given by comparing the ratios, at each temporal frequency, of the response at high contrast to the response at low contrast. In data taken from an LGN X cell [Fig. 3, *top;* replotted from Sclar (1987)], this ratio is relatively constant across temporal frequencies, although slightly larger at higher frequencies. This behavior was fairly typical of 27 X cells studied in Sclar (1987). In two cortical simple cells reported in Albrecht (1995), however (one replotted in Fig. 3, *bottom*), this ratio increases sharply with increasing temporal frequency: higher temporal frequencies give very small responses at low contrast, but reasonable responses at higher contrast. The cortical data for cats is very sparse: we are aware of only the two cells from Albrecht (1995) and one additional cell in Holub and Morton-Gibson (1981) for which temporal frequency tuning at multiple contrasts is reported; all three cells show this effect. The effect is also common, although not universal, in monkey V1 cells [M. Hawken, private communication; Hawken et al. 1992; of 3 published tuning curves, effect is seen in Carandini et al. (1997), Fig. 6 but not Fig. 9 and not seen in Albrecht (1995), Fig. 11], suggesting that a relative boosting with contrast of the high temporal-frequency portion of the temporal tuning curve may be a common V1 property. However, there are no data as to whether, or how strongly, this effect is seen in layer 4 neurons. Moreover, LGN Y cells show a more pronounced c-d boosting of the high-frequency portion of the tuning curve (Sclar 1987) than do X cells. Just as for c-d phase advance, without knowledge of the relative X and Y cell input to studied simple cells, it is unclear how much of this boost, if any, is accomplished by the cortex. We again make the assumption that the cortex must account for the difference in response between X cells and V1 simple cells. Last, these data also suggest, as does one published cell in monkeys (Carandini et al. 1997, Fig. 6), that increases in contrast might also shift the peak of the temporal frequency response curve to higher frequencies.

It is important to note that the relative boosting of high-frequency responses by contrast does not correspond to an increase in contrast gain (the slope of response versus contrast) at higher temporal frequencies. Plotting the responses at each

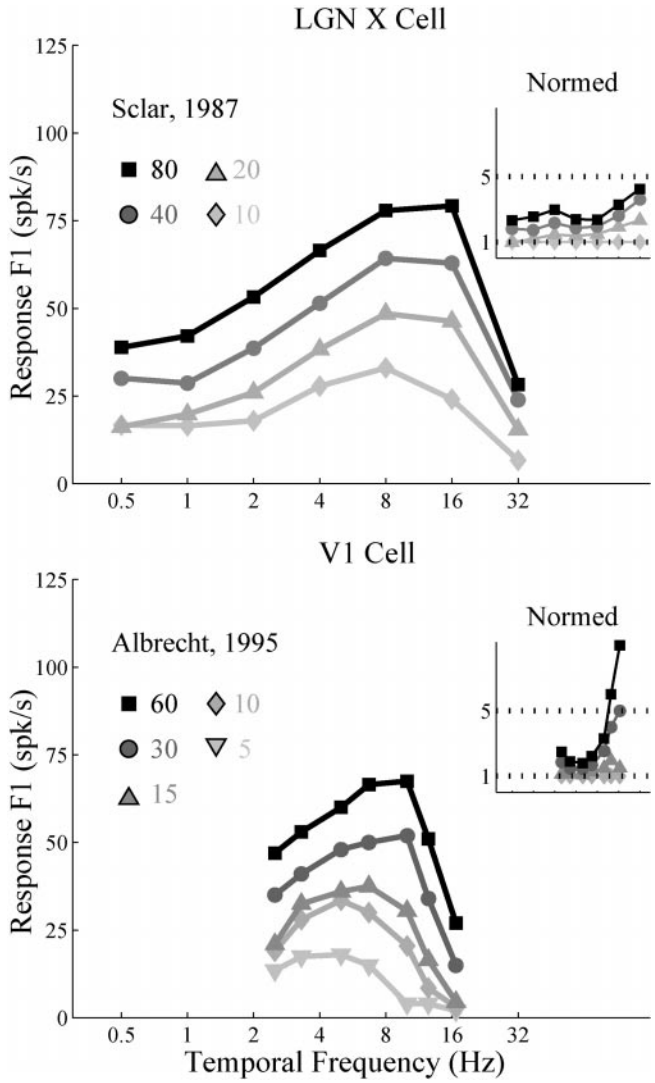

FIG. 3. Contrast enhances responses to higher temporal frequencies more in V1 than LGN. Experimentally determined F1 responses at different temporal frequencies and contrasts for an LGN X cell and a V1 cell. Lighter grays to darker grays, with corresponding symbols: increasing contrast, with values noted in legend for each figure. To show the relative increase in high-frequency responses with increasing contrast, we plot normalized data in the *insets*: each response is divided by the response at the corresponding frequency and 10% contrast (so that all 10% responses are normalized to 1). The 5% V1 cell curves are omitted from the normalized data; we normalize by 10% to better compare to our model curves in Fig. 10 (for which the low contrast is 10%). Dashed lines within the *inset* indicate ratios of 1 (*bottom line*) and 5 (*top line*). LGN X cell temporal frequency response; raw data replotted from Sclar (1987). V1 cell temporal frequency response; raw data replotted from Albrecht (1995).

temporal frequency versus contrast (Fig. 4) makes clear that this slope is not enhanced at higher frequencies and, if anything, is reduced. Another of the three cells in the literature (Holub and Morton-Gibson 1981) showed similar contrast gain at high and low temporal frequencies, but an elevated threshold contrast for higher temporal-frequency responses. Thus the greater relative amplification with contrast of responses to higher temporal frequencies arises because low-contrast responses at higher frequencies are very small, due to lower contrast gain and/or to elevated contrast threshold, and not because high-contrast responses show an elevated contrast gain.

Saturation of responses with increasing contrast

Simple-cell responses tend to reach a plateau with increasing stimulus contrast (Fig. 4, *bottom*); this is known as contrast saturation. This cannot be explained by intrinsic saturation of the cell's ability to fire. As evidenced, for example, by the contrast-invariance of orientation tuning, saturation does not occur at a fixed response level, but rather at different responses levels for different stimuli (so that orientation tuning curves are similar in shape at saturating contrasts and at low contrasts). LGN inputs show contrast saturation as well (Fig. 4, *top*). If LGN input firing does not change with increasing contrast, neither will cortical firing. Thus the question arises of whether cortical saturation level is independent of LGN saturation level.

While the LGN X cell in Fig. 4 indeed saturates at higher contrasts than the cortical cells in that figure, it is not clear whether this is a general phenomenon. Contrast saturation can be measured by a parameter C_{50}: the contrast at which response is half of the maximal, saturating response (determined from a fit of the Naka-Rushton equation, *Eq. A1* in APPENDIX A, to the contrast-response curve). In Table 2, we show the value of C_{50} for the cell of Fig. 4 and for 1 additional cortical and 5 additional LGN X cells for which we found contrast response curves in the literature, along with the mean value reported for over 100 cat cortical simple cells in Albrecht (1995). From these values, it is not obvious whether cortical cells saturate earlier than LGN cells. The same uncertainty applies in monkey, where V1 cells saturate over a range of contrasts similar to the combined saturation ranges of magnocellular and parvocellular LGN cells (Allison et al. 2000; Sclar et al. 1990).

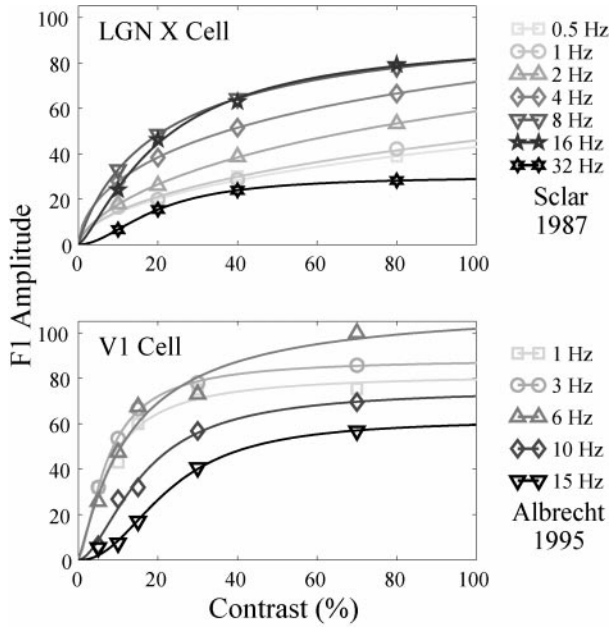

FIG. 4. Experimental data for the temporal frequency dependence of contrast saturation. Experimentally determined F1 responses at different temporal frequencies and contrasts for an LGN X cell and a V1 cell. Figures are replotted from the data shown in Fig. 3, and fitted to Naka-Rushton curves (see APPENDIX A). Lighter grays to darker grays: increasing temporal frequency. LGN X cell contrast saturation response; raw data replotted from Sclar (1987). V1 cell contrast saturation response; raw data replotted from Albrecht (1995). Note that (for the most part, see text and Table 2) the responses of V1 cells saturate at lower contrasts than do the LGN responses, and that cortical responses to higher temporal frequency inputs saturate at higher contrasts.

TABLE 2. *Experimental C_{50} values*

	Temporal Frequency, Hz							
Cell	1	2/2.5	3/3.3	4/5	6/6.7	8/10	12/12.5	15/16/16.7
LGN (1)	>100	>100		>100	35	23.0	21.9	21.8
LGN (2)			12.7					
LGN (3)			14.9					
LGN (4)			6.7					
LGN (5)			8.2					
LGN (6)				5.7				
V1(1)		>100	30.0	16.7	21.6	18.5	28.9	39.1
V1(2)	7.7		7.4		13.1	16.2		22.7
V1 mean					15.5			

C_{50} values from Naka-Rushton curves (*Eq. A1*) fit to experimental data. LGN (1), V1(1), V1(2): cells of Fig. 4, *A–C,* respectively. LGN (2–4): cells from Cheng et al. (1995); LGN (5): cell from Chino et al. (1994). LGN (6): cell from Kaplan et al. (1987). V1 mean: mean from over 100 cat simple cells, each at or near its optimal temporal frequency, reported in Albrecht (1995). LGN (1): temporal frequencies (TFs) 1, 2, 4, 8, 16 Hz. LGN (2–5): TF 3.1 Hz. LGN (6): TF 4 Hz. V1(1): TFs 2.5, 3.3, 5, 6.7, 10, 12.5, 16.7 Hz. V1(2): TFs 1, 3, 6, 10, 15 Hz. For individual cells, we performed least-squares fits of Naka-Rushton curves to published contrast-response data. Best-fit value greater than 100 indicates that the response did not show saturation over the measured contrasts.

However, the phenomenon of contrast adaptation (Albrecht et al. 1984; Ohzawa et al. 1985) strongly suggests a cortical role in setting contrast saturation levels. Sustained presentations of low (high) contrast stimuli shift the cortical response functions to lower (higher) C_{50}s, without corresponding shifts in the LGN response functions. Both threshold and saturating contrasts are shifted by adaptation. This indicates that the cortex can set its saturation level independently of the level at which LGN responses saturate, and motivates us to explore the effects of our model circuit mechanisms on cortical contrast saturation. The strongest components of adaptation operate over time scales longer than that of any mechanism incorporated in our network (mean time to ⅔ of the total effect is 5.5–6.5 s, Ohzawa et al. 1985), so we cannot address these effects. However, contrast adaptation or related phenomena are seen on multiple time scales, including short time scales (Bonds 1991; Geisler and Albrecht 1992; Nelson 1991a,b) that are within the range of mechanisms studied here (spike-rate adaptation, synaptic depression, recruitment of dominant opponent inhibition). Here we address the contributions of these mechanisms to contrast saturation, while noting that other mechanisms might be involved in both saturation and adaptation over longer time scales.

The data on contrast saturation also suggest an additional point that we will address: simple cell responses saturate at higher contrasts as temporal frequency increases. This effect was noted by Albrecht (1995) in discussing the two cells for which temporal frequency tuning was studied at multiple contrasts, and is shown particularly prominently by the cortical cell of Fig. 4. Similar findings have been noted in monkeys (Carandini et al. 1997).

RESULTS

Contrast-dependent phase advance

At least three mechanisms can contribute to cortical c-d phase advance beyond that of the LGN inputs: synaptic depression, spike-rate adaptation, and contrast-dependent increases in conductance. Synaptic depression is evoked by the presynaptic spiking response to the grating stimulus, and differentially suppresses the later portions of the input, and thus of the postsynaptic response, over each stimulus cycle. As illustrated in Fig. 5, this shifts the response peak forward in time. Because the effect of synaptic depression grows with presynaptic firing rate, and thus with contrast, this shift increases with stimulus contrast, yielding a c-d phase advance. Spike-rate adaptation is evoked by postsynaptic rather than presynaptic spiking response, but otherwise it causes c-d phase advance for the same reasons as synaptic depression. Finally, as emphasized in studies of the normalization model (e.g., Carandini et al. 1998; see DISCUSSION), increases in postsynaptic conductance cause a decrease in membrane time constant, and this decrease in integration time causes the phase of responses to advance. If conductance grows with stimulus contrast, this also yields a c-d phase advance.

We first examined the role of synaptic depression. We began by studying the effects of the depression parameters, f (the fraction of synaptic strength remaining after each presynaptic action potential) and τ (the time constant of depression; Fig. 6). Parametric variations of f and τ were carried out only for the geniculocortical synapses: we examined the c-d phase advance of the total geniculocortical input to simple cells in response to optimally oriented spatial gratings drifting at three temporal frequencies. Depression at geniculocortical synapses yields c-d phase advances of 5–10° across a broad range of parameters. We show only rate model results in Fig. 6, as spiking model results are virtually identical.

The dependence of c-d phase advance on f and τ can be understood as follows. A smaller f, representing stronger depression, induces stronger c-d phase advance, up to a point. Once f becomes small enough that the synaptic efficacies are close to zero within the stimulus cycle at some contrast, further increases in contrast have less and less additional effect, so too great a reduction in f can decrease the c-d phase advance (Fig. 6*A*). Smaller τ yields greater recovery from depression between spikes, hence less depression and less c-d phase advance. As τ increases, the depression becomes stronger and the phase advance increases, until τ becomes comparable to the period of the stimulus cycle. At this point, τ is preventing recovery of synaptic efficacy between response cycles. Further increases in τ have little effect on c-d phase advance: such increases change the dynamic range over a cycle, lowering the mean synaptic efficacy and mean response, but do not seem to appreciably alter the time course of depression and recovery

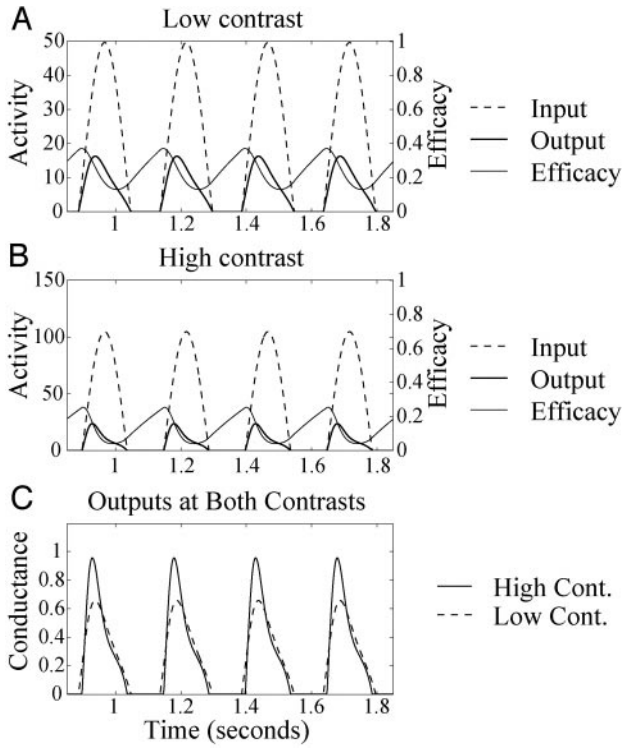

FIG. 5. Geniculocortical synaptic depression induces both an absolute and a relative phase advance. *A* and *B*: steady-state responses to a drifting sinusoidal grating at a cortical cell's preferred orientation and spatial frequency. Dashed lines show firing rate, noted on the ordinate, of a single LGN ON cell input to the cell; thin lines, instantaneous efficacy of the synapse from that LGN input to the cortical cell, normalized by the weight's maximum value; thick lines, conductance contributed by that LGN ON input to the cortical cell, scaled by an arbitrary factor for display purposes (but maintaining the relative difference between low and high contrast conductances across figures). The efficacy decreases as input rate increases, and recovers after input rate declines. Consequently, the peak of the conductance curve, the product of the efficacy times the rate, shifts forward in time relative to the input. This shift in the peak correlates well with the absolute phase advance. The cell's output, which in the absence of intracortical connections is just the LGN conductance temporally filtered by the cell's time constant (and rectified), will show a phase advance similar to that of this single conductance. *A*: responses to a low contrast (10%) stimulus. *B*: responses to a high contrast (80%) stimulus. *C*: comparison of the conductances (now shown unscaled, and measured in Hz) induced by this particular connection at low and high contrast. The steeper and stronger synaptic depression at higher contrast leads to an earlier peak of cortical response in each cycle and thus to a greater phase advance. Depression parameters: $f = 0.465$, $\tau = 371$ ("train" parameters).

within that dynamic range (of course, as $\tau \rightarrow \infty$, the steady-state response level will go to zero, and c-d phase advance will become undefined). Finally, an increase in temporal frequency is roughly equivalent to moving the graphs down and to the left: at higher temporal frequency, there is less time in each cycle for depression to occur, so a larger f is needed to get an equivalent amount of depression, and there is less time in each cycle to recover from depression, so a smaller τ gives an equivalent amount of recovery.

Next, for fixed f and τ (set either according to the pulse or train parameters, Table 1), we examined the relative contributions of synaptic depression at different synaptic loci in the full model circuit, using the rate model. This model has no spike-rate adaptation and has a fixed membrane time constant, so only depression should contribute to the c-d phase advance. Synaptic depression can be found in any of three locations: in the geniculocortical synapses (G), in the intracortical excitatory synapses (E), and in the intracortical inhibitory synapses (I). This yields eight possible configurations for the locations of depressing synapses. Depression in the I synapses had little effect on phase advance, so we illustrate the c-d phase advance produced by the four configurations not involving I as well as for the case of depression at all locations (Fig. 7). Matching these data across the different depression conditions is not trivial; one must ensure that the data are comparable by matching firing rates, for example, or by using the same set of parameters in all cases. We chose to show the distribution of results for all model parameter sets that satisfied the known experimental constraints (see APPENDIX A) at a given temporal frequency. Similar plots in which we include only model parameter sets that fit the constraints at *all* temporal frequencies give similar results with less variability, but there are no such parameter sets within our search range for some cases (both sets of "G" cases, and the train "E" case).

As evidenced by Fig. 7, depression of either geniculocortical or intracortical excitatory synapses can induce approximately 5° of c-d phase advance, and these advances sum when depression is present in both locations. In the absence of any depression, there is no c-d phase advance, as expected. These general results are for the most part similar across temporal frequency of the input and choice of synaptic depression parameters (pulse vs. train), except that the train parameter set tends to produce somewhat larger phase shifts than the pulse set, as is also evident in Fig. 6.

To consider the additional effects of spike-rate adaptation and of contrast-dependent changes in membrane time constant, we turn to the spiking model. In this model, depression was included only at geniculocortical synapses, for reasons described in APPENDIX A. In the absence of depression ("D") or adaptation ("A"), a c-d phase shift of 3–4° appears, increasing slightly with temporal frequency (Fig. 8, "No A, No D"). This is roughly consistent with the observed contrast-induced decreases in membrane time constant.[1] Adding either adaptation alone ("A, no D") or geniculocortical depression alone adds roughly another 5°, and the effects of these two mechanisms together are additive.

With all three mechanisms present, the spiking model shows mean c-d phase advance of 13–15°, relative to LGN, for either set of depression parameters (Fig. 8). Depression in intracortical excitatory synapses can easily add another 5° (Fig. 7). This suggests that these mechanisms may be sufficient to account for the roughly 20° difference between LGN X cell and V1 c-d phase advances that have been observed in cats (Fig. 2). However, while we have found that the effects of geniculocortical depression add with those of intracortical E depression (Fig. 7) and with those of adaptation (Fig. 8), we

[1] The time constant τ varies across a stimulus cycle, but a simple analysis can be obtained by regarding τ as fixed for a given contrast. Then the formula for contrast-dependent phase advance, in units of time, is $[\arctan(2\pi f\tau_0) - \arctan(2\pi f\tau_1)]/2\pi f$, where τ_0 and τ_1 are the low-contrast and high-contrast time constants, respectively, and f is temporal frequency. Including the effects of stimulus-independent background firing, τ in the spiking model is approximately 15 ms in the absence of a stimulus, 12.5 (DC) ± 1.5 (F1) ms for F1 = 30 flat LGN inputs, and 8 (DC) ± 2.5 (F1) ms for F1 = 90 flat LGN inputs. A change of τ from 12.5 to 8 ms or from 14 to 10.5 ms [mean or (mean + F1)] would predict advances of 2.5 or 3° at 2 Hz and 7 or 10° at 8 Hz. The prediction is worse at higher temporal frequencies, but the assumptions may also be more problematic since conductance changes more rapidly at higher frequencies.

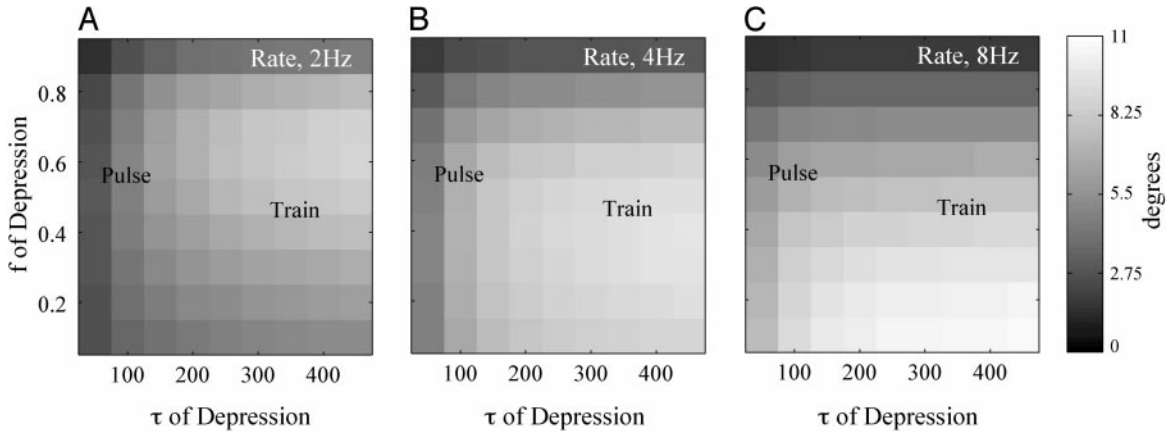

FIG. 6. The dependence of contrast-dependent geniculocortical phase advance on f and τ in the rate model, shown for drifting gratings of (*A*) 2-Hz, (*B*) 4-Hz, and (*C*) 8-Hz temporal frequency. Black indicates less phase advance; white indicates more phase advance. The experimental values of the geniculocortical f and τ parameters for the pulse and train data sets (Table 1) are marked by the words "Pulse" and "Train." Gratings were of optimal orientation and spatial frequency; mean c-d phase advance across simple cells of multiple spatial phases is shown. In this figure, response is simply the summed geniculocortical input to simple cells, ignoring cortical integration; thus results are independent of choices of cortical model parameters. c-d phase advance is measured for the sum over a cell's geniculocortical inputs of synaptic efficacy times firing rate. Results are extremely similar for geniculocortical input currents in the spiking model (not shown), with small differences due to the Poisson sampling of firing rates in the latter model; depression in the rate model should correspond to average over Poisson samples (see APPENDIX B).

have not studied the three together. We tried modeling adaptation in the rate model, but did not see an effect on c-d phase advance. In our simple rate model, adaptation was proportional to the rate, and therefore was active even at low rates. In reality and in our spiking model, the net effect of adaptation increases faster than linearly with firing rate: the mean adaptation current increases proportionally to the rate, but the effect of this current on spiking increases with rate, because at higher rates (smaller interspike intervals), there is less time for the spike-induced current to decay between spikes. This difference appears to be critical to the c-d phase advance induced by adaptation. Rather than include a more complicated (and underconstrained) dependence of adaptation on rate, we elected to study only the effects of synaptic depression in the rate model, and to study adaptation only in the spiking model. Conversely, as discussed in APPENDIX A, for reasons of computational complexity, we did not study depression of intracortical synapses in the spiking model.

We also examined the dependence of phase shift on stimulus orientation in the rate model (data not shown). c-d phase advance remains essentially constant across orientations that give reasonable response.

Contrast-dependent changes in temporal frequency tuning

We next studied the contrast dependence of temporal frequency tuning. As in our studies of c-d phase advance, we wanted to isolate the cortical contribution to temporal frequency tuning; in this case, to understand the cortical response in the absence of any incoming temporal information beyond the stimulus-driven temporal modulation of the input rates. Experimentally, the LGN inputs show temporal-frequency dependence in the amplitude of their rate modulations (response F1; Fig. 3, *top*). Thus we found it convenient to consider an even simpler model of LGN responses, in which the LGN response F1 was constant across temporal frequencies at a given contrast, with larger F1s representing higher contrast. We refer to such an LGN response profile as "flat," in distinction to the experimental tuning of Fig. 3, *top*, which we refer to as "Sclar" tuning [because the experimental data are from Sclar (1987)]. Using flat LGN tuning, we can examine cortical contributions to temporal tuning; we can then examine full cortical responses using Sclar LGN tuning.

Assuming flat LGN tuning, there are at least four cortical factors that contribute to temporal frequency tuning and its contrast dependence: *1*) the cellular time constant and its decrease with increasing stimulus contrast; *2*) the spike-threshold nonlinearity; *3*) spike-rate adaptation; and *4*) synaptic depression. We consider the effects of each of these in turn.

Cellular (and synaptic) time constants act as low-pass filters, causing the modulation of the simple cell's voltage response (the 1st harmonic of F1 of the voltage response) to decrease with increasing temporal frequency.[2] As we have already noted, the average membrane time constant of a cortical cell shrinks as the amount of synaptic input to the cell increases, because increasing synaptic drive increases membrane conductance. As a result, at higher contrasts the voltage responses to higher temporal frequencies are less attenuated by cellular filtering than at lower contrasts (Carandini and Heeger 1994). This effect is captured in the spiking model, but not in the rate model which has a fixed time constant. The effect is modest: the mean time constant in the spiking model shrinks from 12.5 to 8 ms between the low (F1 = 30) and high (F1 = 90) flat input levels (further details in footnote 1). Assuming a linear model of voltage response, this yields about an 18% increase in the high-contrast voltage F1 at 12 Hz relative to that expected from the low-contrast time constant.

However, this modest effect can become significant when combined with the nonlinearity of a nonzero spiking threshold:

[2] A linear model of a cell with time constant τ produces modulated first harmonic responses to temporal frequencies f proportional to $1/\sqrt{1 + (2\pi f\tau)^2}$; $f = 1/\tau$; diminishes the maximum response by 84%. Membrane time constants of 8–16 ms, as used in the rate model, would produce corresponding attenuations of 14–35% at 12 Hz, and 22–46% at 16 Hz, relative to responses at 2 Hz. The time constant in the spiking model covers a similar range (footnote 1).

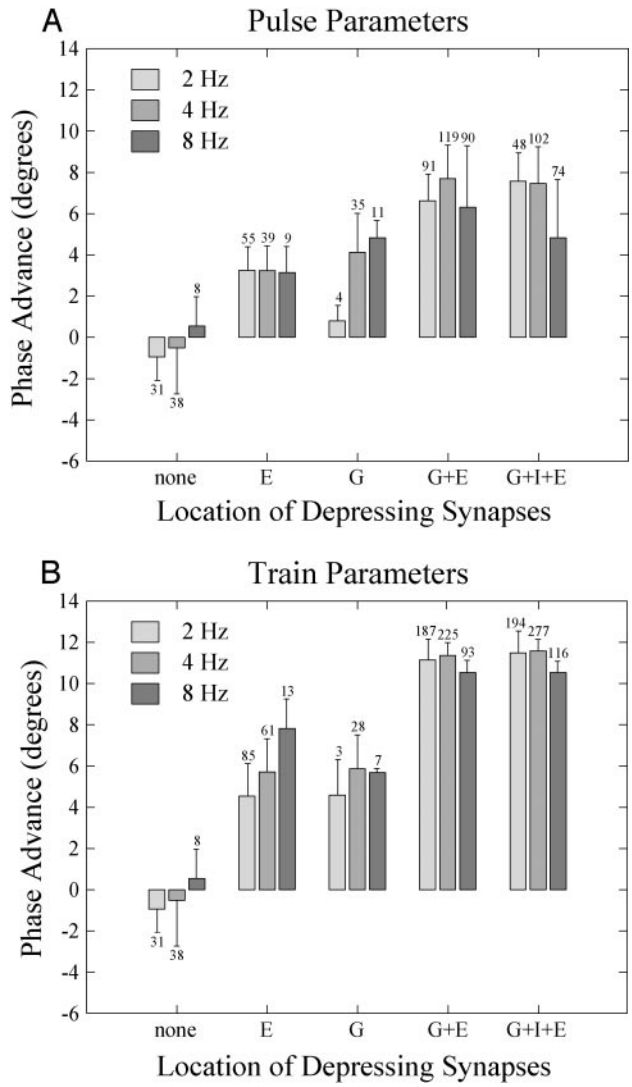

FIG. 7. Dependence of c-d phase advance on the location of depressing synapses. Graphs show c-d phase advance ± SD for those rate model parameter sets that produce constraint-satisfying outputs (see APPENDIX A) at a given temporal frequency. The number of parameter sets contributing to each data point is noted above each error bar. c-d phase advance is shown for grating inputs with temporal frequencies of 2, 4, and 8 Hz, represented by the light gray, gray, and dark gray bars, respectively. The location of the depressing synapses, if any, in each of the cases is indicated by the letter(s) on the abscissa (G = geniculocortical, I = inhibitory, E = excitatory intracortical). The 3 bars above "G + I + E," for example, indicate the c-d phase advance ± SD for 2-, 4-, and 8-Hz grating inputs when the rate model includes depression in all 3 of the G, I, and E synapses. *A*: c-d phase advance for "pulse" depression parameters. *B*: c-d phase advance for "train" depression parameters. Note that the rate model is completely deterministic; the SDs arise from the averaging of all constraint-satisfying parameter sets for the given temporal frequency and location(s) of depressing synapses. When we restricted ourselves to parameter sets that satisfied constraints across all 3 temporal frequencies, results were very similar where such parameters were found (except that SDs were much smaller); but no such sets were found for some locations of depressing synapses (see text).

the threshold gives rise to an "iceberg" effect. Figure 9*A* shows responses in the spiking model to four levels of flat LGN input, when adaptation but not depression is present. At 12-Hz input frequency, the response is close to zero for input F1s of 15 or 30 spikes per second, but thereafter grows with increasing input F1, suggesting a threshold effect. This can be confirmed by viewing the corresponding intracellular voltage traces for a randomly chosen cell with spiking turned off (Fig. 9*B*); the spike threshold of −52.5 mV is indicated as a dashed line. The modest attenuation of voltage modulation due to membrane filtering is, on average, sufficient to keep voltage responses subthreshold at the lower input levels. Higher input modulation levels, however, yield higher voltage modulations that consistently cross threshold. This threshold effect depends on our circuit model, in which inhibition is dominant so that the mean response to a sinusoidal grating is always subthreshold and spiking occurs only on voltage modulations (Troyer et al. 1998); in a model in which the mean input to a preferred stimulus was suprathreshold, the modest affects of cellular filtering on the voltage modulations would have only modest effects on spike response.

To examine the effects of the other mechanisms, we examined temporal frequency tuning curves with and without synaptic depression (Fig. 10: *A*, no depression; *B*, pulse depression parameters) and, for the spiking model, with and without

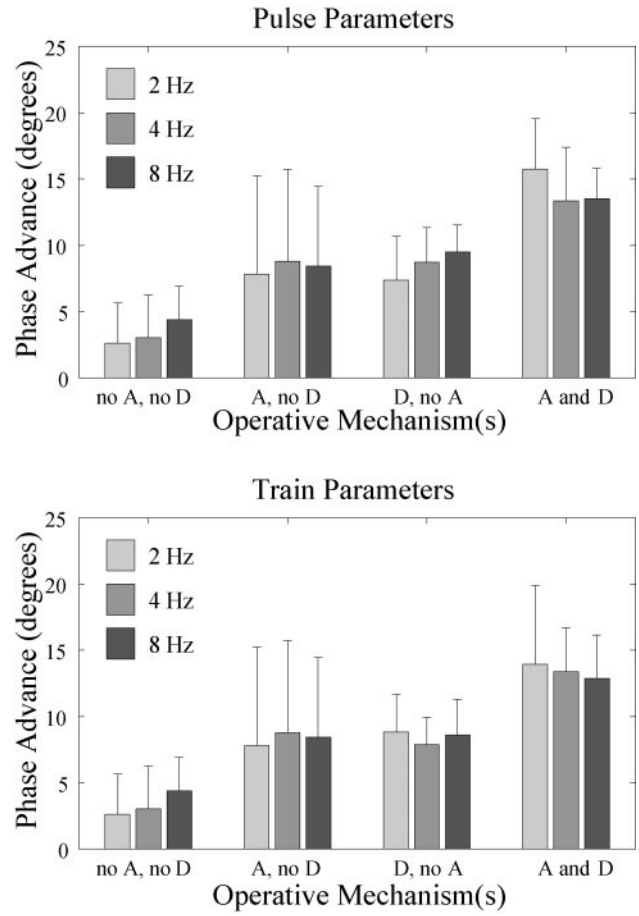

FIG. 8. c-d phase advance of spiking model in the presence of different temporal nonlinearities for different temporal frequencies of input. Light gray: input gratings at a temporal frequency of 2 Hz; gray: input gratings at 4 Hz; dark gray: input gratings at 8 Hz. Four different types of simulations were run: from *left* to *right*, simulations with neither spike-rate adaptation nor synaptic depression ("no A, no D"), simulations with only spike-rate adaptation ("A, no D"), simulations with only synaptic depression ("D, no A"), and simulations with both mechanisms present ("A and D"). We calculated a c-d phase advance from the peristimulus time histograms for each of the 29 cells examined, then computed the mean and SD across cells for each condition. Both spike-rate adaptation and geniculocortical synaptic depression induce a c-d phase advance, and the advance increases when both are present simultaneously.

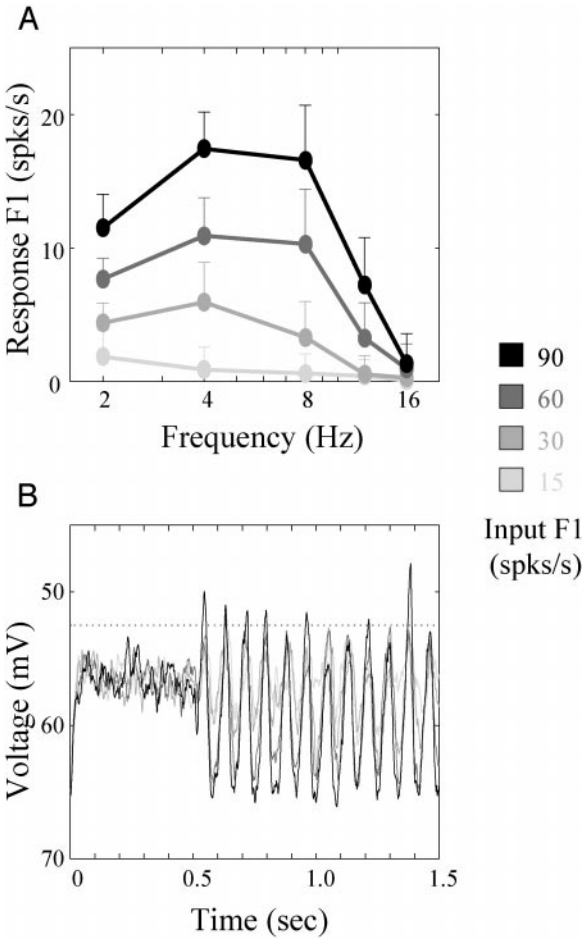

FIG. 9. The iceberg effect: the appearance of higher temporal frequency responses at higher contrasts. *A*: temporal frequency tuning curves for "flat" F1 inputs of 15, 30, 60, and 90 Hz (prerectification values), color-coded from light gray to black, respectively, for a spiking model simulation in which adaptation was present, but synaptic depression was not. Error bars indicate SDs of the means across 29 cells. Note that responses to 12-Hz input gratings are present for input F1s of 60 and 90 Hz, but essentially absent for input F1s of 15 and 30 Hz. Input F1 of 30 Hz corresponds roughly to 10% contrast, 90 Hz roughly to 80% contrast (see Fig. 10). *B*: intracellular voltage traces, for a randomly chosen cortical cell, in response to a single presentation of a 12-Hz temporal frequency grating at each of the 4 F1 input levels used in *A* (corresponding, at 12 Hz, to contrasts of 3.9, 7.8, 18.7, and 41.2%). Spiking responses in the cell have been turned off; spiking threshold is indicated by the dotted line. Synaptic conductances for LGN inputs and nonspecific in vivo "back-ground" inputs (see APPENDIX A) were turned on at *time 0*. A blank stimulus was presented for the 1st 0.5 s of the trace, after which the grating stimulus appeared. Note that, for input F1 values of 15 or 30 Hz, the membrane voltage never crossed spike threshold. For higher input F1 values (60 or 90 Hz), the membrane potential did reach threshold, as corroborated by the increase in the spiking response indicated in *A*. Traces were achieved as follows: all conductances onto a cell, including spike-rate adaptation conductances, were recorded during simulations of *A*. These conductances were then "played back" to the cell with spiking turned off.

spike-rate adaptation currents (Fig. 10, spiking model: *middle panels*, no adaptation; *bottom panels*, with adaptation). In all cases, we present data for both flat (dashed lines in Fig. 10) and Sclar (solid lines in Fig. 10) LGN tuning. The *top panels* of Fig. 10, *A* and *B*, show the LGN input to simple cells. LGN cells respond better to high than to low temporal frequencies and show slightly more contrast-dependent enhancement of both high and low temporal frequencies than of middle temporal frequencies (Fig. 10*A*, Sclar inputs). In the absence of depression or adaptation, the filtering by the cortical cell's membrane time constant, combined with the spike threshold, produces strongly low-pass cortical responses (Fig. 10*A*, *middle panels*). Both spike-rate adaptation (Fig. 10, *bottom panels*) and synaptic depression (Fig. 10*B*) suppress responses to lower-frequency stimuli much more strongly than responses to higher-frequency stimuli, and can convert low-pass cortical response into a more band-pass response. This property of synaptic depression also virtually eliminates the difference between flat and Sclar inputs (Fig. 10*B*, *top panels*). Train parameters for synaptic depression produce results similar to pulse parameters, except that there is less difference between responses to low versus high contrasts (not shown).

Both synaptic depression and spike-rate adaptation contribute to the relative enhancement of higher temporal-frequency responses at high contrast. Each is more strongly activated by higher-contrast than by lower-contrast stimuli, and each more strongly suppresses responses to lower-frequency than to higher-frequency stimuli. These contrast-dependent effects are most clear in the "normed" *insets* in each panel of Fig. 10, which show the ratio of high-contrast to low-contrast responses versus temporal frequency. This ratio strongly increases at higher temporal frequencies for cortical responses in every case except for that of the rate model without depression (Fig. 10*A*). That case is the only one that lacks any of the three mechanisms of contrast-dependent changes in membrane time constant, synaptic depression, and spike-rate adaptation. Adding depression alone (Fig. 10*B*, rate model) or membrane time constant changes alone (Fig. 10*A*, spiking model, no adaptation) suffices to give contrast-dependent enhancement of high-frequency responses. Addition of spike-rate adaptation in the spiking model tends to eliminate any relative enhancement of lower frequencies while preserving such enhancement at higher frequencies. Synaptic depression also suppresses the contrast-dependent differences between LGN input conductances, making different contrasts appear more alike to the cortical cell. This reduces the strength of contrast-dependent response enhancement at all temporal frequencies.

We see at best only a weak shift in the peak of the temporal frequency tuning curve with increasing contrast. At present, there are no experimental data as to whether LGN-recipient cells in cat layer 4 show such a shift in peak. If they do not, but instead show only a relative increase in responses to higher temporal frequencies at higher contrast, this could be sufficient to induce shifts in the tuning peaks of downstream cells.

Saturation of responses with increasing contrast

Last we examined the saturation of cortical responses with increasing contrast (Fig. 11). Even in the absence of depression or spike-rate adaptation, model cortical responses tend to saturate somewhat earlier than their LGN inputs, particularly at lower temporal frequencies (Fig. 11*B*). If either pulse or train depression is active, saturation occurs significantly earlier than in either the LGN inputs or the models without depression. (The one exception is at the highest temporal frequency of the spiking model, for which responses are small and the measure of saturation probably inaccurate.) Moreover, clearly in the depression cases, and also somewhat in the examples lacking depression, there is a tendency for responses to higher temporal frequencies to saturate later than responses to lower temporal

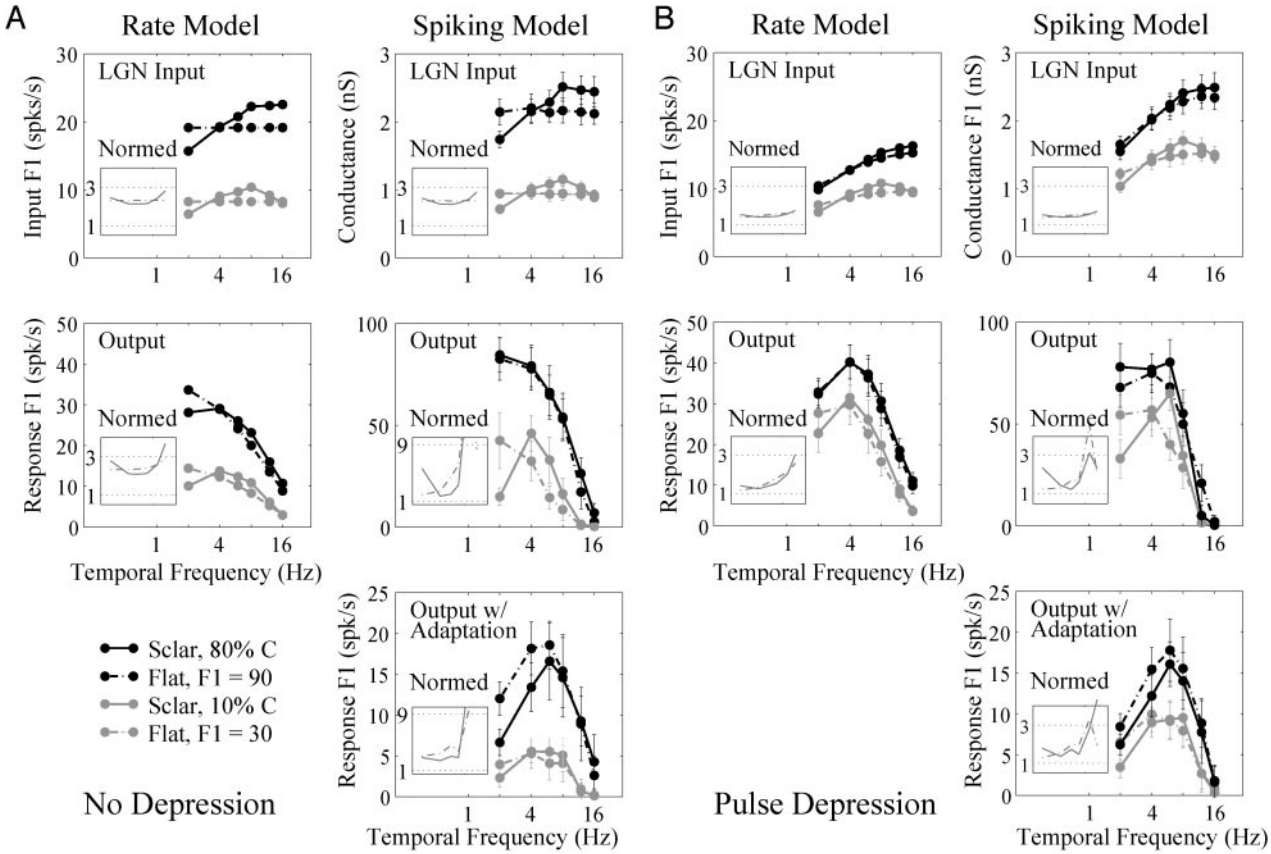

FIG. 10. The contrast dependence of temporal frequency tuning for different outputs of the rate and spiking models. *X*-axes: temporal frequency. *Y*-axes: for *top rows*, F1 of summed LGN input to a simple cell (measured in Hz for the rate model and in nS for the spiking model); for all other plots, F1 of excitatory simple cell firing response, measured in spikes per second. Two types of LGN inputs were used. Model responses to "flat" LGN inputs are indicated by dashed lines; responses to experimentally measured "Sclar" LGN inputs, Fig. 3*A* (Sclar 1987), are indicated by solid lines. Gray lines show responses to 10% contrast ("Sclar") or LGN response F1 of 30 ("flat"), while black lines indicate responses to 80% contrast or F1 of 90. Note that the F1 values of the flat inputs are set before LGN outputs are calculated; i.e., they are "prerectification" values (see APPENDIX A). *Insets*: responses at high-input level divided, frequency-by-frequency, by low input level responses. For each of *A* and *B*: *left column* shows rate model, *right column* spiking model; *top row* shows LGN input to simple cell, *middle row* shows simple-cell firing responses without spike-rate adaptation currents, and *bottom row* shows simple-cell spiking responses with spike-rate adaptation currents in excitatory cells (spiking model only). *A*: no synaptic depression. *Top row*: because depression is absent, conductances very closely follow the temporal frequency dependence of LGN response amplitudes. *Middle row*: because of filtering by the membrane time constant at higher, but not lower, temporal frequencies (see text), as well as inhibition in the model circuit, both types of model show low-pass behavior, as well as a relative amplification of high temporal frequency responses with contrast (*insets*). *Bottom row*: note the band-pass nature of the response induced by spike-rate adaptation, in addition to the relative amplification of high temporal frequencies (*inset*). Note that *bottom row*, dashed lines of *A* is the same data as in Fig. 9 for F1 = 30 and F1 = 90. *B*: "pulse" depression. *Top row*: with depression present, LGN input conductances no longer closely follow the temporal frequency dependence of LGN response amplitudes; low-frequency responses show a relative attenuation, even for "flat" inputs. *Middle, bottom rows*: cortical outputs are correspondingly band-pass and show relative amplification of high temporal frequencies. Rate model plots include results only for parameter sets that satisfied experimental constraints (see APPENDIX A) at every temporal frequency. There was 1 parameter set for no depression and 3 for pulse depression (plots show average over parameter sets). Depression in the rate model was incorporated at all synapses (G + I + E, Fig. 7). In all cases, spiking model results show averages over 29 cells. All error bars indicate SDs.

frequencies: for cases with depression, C_{50} values increase monotonically with temporal frequency if the lowest temporal frequency is excluded. The same pattern is seen in the V1 cell of Fig. 4, although the model C_{50} values are somewhat lower than those measured by Albrecht.

The contrast saturation effects induced by synaptic depression can be readily understood. As demonstrated by Abbott et al. (1997) and Tsodyks and Markram (1997), in the presence of depression, as a presynaptic neuron's firing rate increases to values much larger than $1/\tau$ (where τ is the time constant of recovery from depression), the overall postsynaptic effect of its synapses (proportional to rate times efficacy) saturates at a plateau value. The postsynaptic cell cannot "see" further increases in rate. Thus as LGN firing rates increase with contrast, the impact on the cortical cells will plateau earlier than it would without depression. This saturation occurs at higher contrasts for higher temporal frequencies, because depression more strongly suppresses lower than higher-frequency inputs.

As can be seen in the table, however, cortical responses can saturate at lower contrasts than LGN even when depression is absent. This results from the inhibition in our circuit model. Because the cortical response is determined by a thresholded version of the membrane voltage, for a sinusoidal input grating the response of the cortex can be largely understood from the

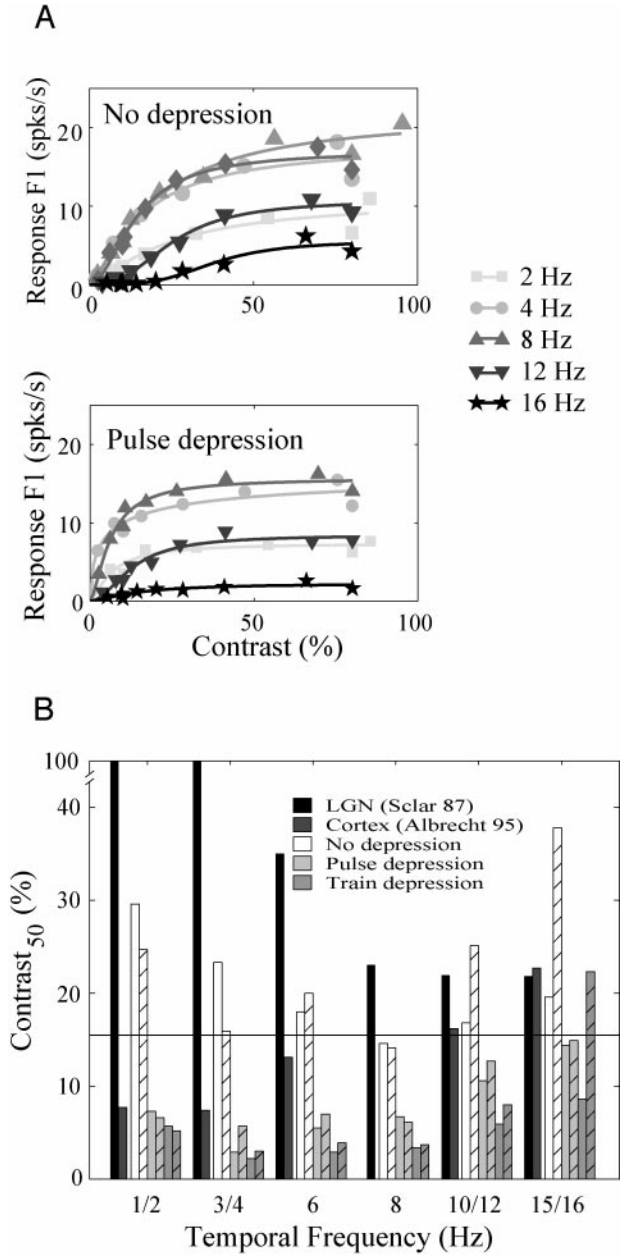

FIG. 11. Model data for the temporal frequency dependence of contrast saturation. *A*: model contrast saturation curves for spiking model (averages over 29 cells) with spike-rate adaptation, with no depression and with pulse depression. Light gray to dark gray: increasing temporal frequency. *B*: saturating contrast (C_{50} in fit of Naka-Rushton curve to contrast saturation curve) vs. temporal frequency for LGN cell (Sclar 1987) and cortical cell (Albrecht 1995) of Fig. 4 (dark bars) and for model cells with no depression, pulse depression, or train depression (white, light gray, dark gray) in rate model (solid bars) or spiking model (hatched bars). Horizontal line shows mean C_{50} from over 100 cat V1 simple cells, each at or near its optimal temporal frequency, reported in Albrecht (1995). Results for pulse and train depression are qualitatively similar. As described in the text, cortical responses tend to saturate at lower contrasts than do their LGN inputs, and responses to higher temporal frequencies saturate at higher contrasts. Depression in the rate model was incorporated at all synapses (G + I + E, Fig. 7).

peak membrane voltage. We estimate this peak as the sum of the mean voltage and the modulation amplitude, or first harmonic, of the voltage. In the absence of inhibition, this peak voltage closely follows the modulation of the LGN input: tuning curves of peak voltage and of LGN modulation show very similar C_{50}s under various conditions (data not shown). However, when inhibition is added, the peak voltage can show C_{50} values that are lower than the corresponding LGN values, because the inhibition in the model both decreases the slope of, and adds a constant negative DC offset to, the curve of peak voltage versus contrast. The DC offset originates from the background firing of the LGN, which, because the cortex is inhibition dominated, is net inhibitory. By both flattening and shifting the cortical response curve closer to zero, inhibition effectively causes cortical neurons to saturate sooner than their inputs.

DISCUSSION

We have established that a simple circuit model of cat layer 4 that achieves contrast-invariant orientation tuning can also account for three c-d nonlinearities in simple cell responses to sinusoidal stimuli: c-d phase advance, c-d changes in the shapes of temporal-frequency tuning curves, and contrast saturation. These response nonlinearities arise locally (that is, in a circuit in which both excitatory and inhibitory intracortical connections are primarily between cells of nearby preferred orientations) as a result of the many nonlinear elements present in the LGN responses and cortical circuitry. The observed c-d phase advance can be largely or entirely accounted for by the combined effects of geniculocortical and intracortical synaptic depression, spike-rate adaptation currents in cortical cells, and c-d changes in cortical cell conductance. The greater ratio of high-contrast to low-contrast responses for high versus low temporal frequencies arises from the interaction of these nonlinearities with the spike threshold, along with the dominance of inhibition in our model circuit. Finally, the inhibition in our model circuit causes cortical cell responses to saturate at slightly lower contrasts than do the LGN inputs, while synaptic depression causes a much stronger decrease in cortical saturating contrast relative to LGN.

These results were derived in the context of a circuit model that has previously been shown to account for a wide variety of observations related to orientation tuning in cat layer 4 (Troyer et al. 1998). However, only some of the present results depend on this circuit model. The circuit model was critical to establishing that the c-d nonlinearities studied here could coexist with the more linear-like behavior of contrast-invariance of orientation tuning. In addition, the relationships of inhibition and excitation in the circuit model are critical to the threshold effect underlying the c-d changes in temporal frequency tuning: it is crucial that inhibition is dominant so that the mean input is subthreshold, since suprathreshold mean input would cause small changes in input modulation to have only small effects on responses; and it is crucial that inhibition is spatially opponent to excitation, so that excitation can periodically drive responses to a preferred-orientation grating despite this overall dominance of inhibition. The circuit model used is not critical to the mechanisms of c-d phase advance and contrast saturation explored here, although the inhibition in the model circuit does contribute to contrast saturation.

Coexistence of linear and nonlinear response properties

We have emphasized that it is important not simply to explain nonlinear response properties, but to understand how

they can coexist with "linear-like" properties such as contrast-invariant orientation tuning. In particular, how can the circuit show contrast invariance in the tuning for orientation at each temporal frequency, and yet show contrast dependence in the tuning for temporal frequency at the preferred orientation?

The answer is that key nonlinearities within the circuit vary with temporal frequency, but not with orientation. As noted previously, each grating presented to the circuit gives rise to both a mean voltage and a voltage modulation about that mean. A change in orientation away from the preferred does not alter the mean input to a cell, but only decreases the input modulation. The contrast-induced growth in the mean response is converted into inhibition that offsets the concomitant growth in the modulations, which is roughly proportional across orientations, yielding contrast-invariant orientation tuning. The situation is different for temporal frequency: both the mean and the modulation of the input are altered by a change in temporal frequency. Synaptic depression strongly suppresses the input mean relative to the input modulation at low temporal frequencies, but not at higher temporal frequencies (Krukowski 2000). Furthermore, an increase in stimulus contrast causes greater amplification of input modulations at higher versus lower temporal frequencies, because of c-d decreases in membrane time constant as well as depression and spike-rate adaptation. Finally, LGN input firing rates show a slightly greater contrast-dependent increase at high than at low temporal frequencies. Thus the contrast invariance of orientation tuning and the contrast dependence of temporal frequency tuning follow from the frequency- but not orientation-dependent nature of the circuit nonlinearities.

Limitations of the present work

Several of our explanations depend on the existence of sufficient synaptic depression in vivo. One study reported that cortical depression appears weaker in vivo than in vitro (Sanchez-Vives et al. 1998), but speculated that this may result simply from the greater baseline rate of depression in vivo due to background activity, an effect included in our modeling. Support for a functional depression-like mechanism in vivo was reported by Nelson (1991a,b): responses in cat V1 were suppressed by repetition of visual stimuli in a manner consistent with both synaptic depression and a presynaptic origin. We attempted to control for the uncertainty in the strength of depression by studying two different in vitro parameter sets; they showed little difference in behavior except that the train parameters reduced the difference between low- and high-contrast response amplitudes.

The model weakly suggests that geniculocortical depression may be less strong than in either of these parameter sets. Geniculocortical synaptic depression with these parameters, and particularly with the train parameters, led model cells to saturate too early, relative to cortical cells (Fig. 11). However, nonlinearities in LGN temporal response profiles beyond the simple rectification considered here might alter this result. In particular, LGN responses tend to occur over significantly less than a half-cycle of a sinusoidal stimulus (e.g., Reich et al. 1997); this would be likely to affect response saturation similarly to going to a higher temporal frequency, for which saturation occurs at higher contrasts.

The similarity of results in both the simpler rate model and the more elaborate spiking model, and the ability to understand their differences in terms of the specific additional nonlinear mechanisms present in the spiking model, give confidence that the understandings achieved here of the contribution of each nonlinear mechanism to each nonlinear response property are fairly robust; i.e., independent of specific implementation. Further mechanisms not considered here may also play a role, such as further nonlinearities in LGN responses, other active membrane conductances beyond spike-rate adaptation (McCormick 1990), nonlinearities of dendritic integration (e.g., Larkum et al. 1999), synaptic facilitation, which is seen at many excitatory synapses onto inhibitory interneurons (Thomson et al. 1993), or the presence of NMDA receptors, which can alter temporal frequency tuning in our model (Krukowski 2000). These uncertainties limit our ability to make strong quantitative predictions. But the present results establish the viability of a local explanation of contrast-dependent nonlinearities, and they allow qualitative tests, discussed further below.

Applicability of the model to other species

Contrast-dependent nonlinearities have also been studied in monkeys. Data there, although also limited, seem qualitatively consistent with those in cats (Albrecht 1995; Carandini and Heeger 1994; Carandini et al. 1997; Hawken et al. 1992). However, response properties in the LGN-input-recipient portions of monkey layer 4 are quite different from those in cat layer 4: while cat layer 4 consists very largely of classical simple cells [cells with aligned and oriented, segregated ON and OFF subregions and strong orientation tuning (Bullier and Henry 1979; Gilbert 1977)], monkey layer 4C has few such cells (Blasdel and Fitzpatrick 1984; Hawken and Parker 1984). Thus our model circuit is unlikely to apply directly to monkeys. As we discussed above, many of our explanations of c-d nonlinearities are independent of the circuit studied. In the cases where the circuit plays a role, the critical elements of the circuit are the dominance of inhibition and its opponency with excitation. We have conjectured that these may be general principles of cortical layer 4 circuitry (discussed in Troyer et al. 1998), and so in particular might also characterize layer 4 of monkey V1.

Experimental tests of the model

The present explanations of c-d phase advance can be directly tested by blocking spike-rate adaptation and/or synaptic depression and determining whether this decreases c-d phase advance. Spike-rate adaptation can be blocked by several pharmacological agents (Baskys 1992; Nicoll 1988). If applied iontophoretically to individual cells, these should reduce c-d phase advance [although spike-rate adaptation may not be as strong in vivo as in vitro (Tang et al. 1997)]. Selective intervention against synaptic depression is more difficult (see Discussion in Chance et al. 1998).

The combined role of LGN response nonlinearities and geniculocortical synaptic depression in both c-d phase advance and contrast saturation could be assayed in intracellular recordings from simple cells, by using electrically evoked cortical suppression (Chung and Ferster 1998) to isolate geniculocortically driven currents during presentation of sinusoidal grating stimuli. By comparing c-d response properties of these input

currents to those of the cell's voltage response with the cortical circuit intact, the degree of involvement of cortical mechanisms could be assessed. Comparisons to average LGN firing properties might be used to assay the role of geniculocortical synaptic depression; we would predict that these input currents would show greater c-d phase advance and earlier contrast saturation than LGN firing rates.

The explanation of c-d changes in temporal frequency tuning could be tested by measurements of the membrane potential in response to high-temporal-frequency gratings of increasing contrast. In cells showing a c-d change in the shape of temporal frequency tuning curves favoring higher temporal frequencies, we predict a threshold effect: as contrast increases, the spiking response should increase faster than the voltage response.

Other experimental work suggested by the model

As we emphasized in the section on EXPERIMENTAL FINDINGS ADDRESSED, the data on response nonlinearities remain quite sparse. None of the data in cats are known to be from layer 4 (although most are from identified simple cells); it will be important to determine the degree to which layer 4 cells exhibit these nonlinearities. LGN Y cells show stronger response nonlinearities than X cells, emphasizing the importance of correlating nonlinear cortical response properties to the proportion of X or Y input received by a cell. LGN and cortical response nonlinearities have not been studied under the same conditions or in the same animal, with the exception of one study in monkeys (of contrast saturation, Sclar et al. 1990). This is particularly important for temporal response properties, which may be quite mutable by different types of anesthesia: increases in inhibition, as induced by barbiturates, can cause a lower temporal frequency cutoff in responses at a given contrast in our circuit model, while blockade of NMDA receptors, e.g., by ketamine, can have variable effects on temporal frequency tuning (Krukowski 2000).

Further data on the dependence of c-d phase advance on temporal frequency and stimulus orientation, particularly in cat layer 4, could limit potential parameters and mechanisms. Albrecht (1995) reported a weak positive correlation between c-d phase advance and temporal frequency across cat and monkey simple cells. We do not see such dependence in our average results, but individual parameter sets can show such dependence (e.g., Fig. 6). Similarly, data for a few cells in monkey V1 (Carandini et al. 1997) showed little dependence of c-d phase advance on stimulus orientation. While average phase advance in the rate model showed no dependence on stimulus orientation for orientations that give appreciable response, we have not carefully examined the parameter dependence of this result, and orientation dependence would be expected for components of c-d phase advance due to adaptation or conductance changes, which were not included in the rate model.

Comparison to other models

The importance of understanding the nonlinearities studied here has been emphasized by studies of the normalization model (Albrecht and Geisler 1991; Carandini et al. 1997, 1998; Heeger 1992). These studies have strongly influenced the field's thinking: as a phenomenological description of cortical processing, the normalization model integrates a wealth of data in a simple way.

However, as a mechanistic explanation, this model is problematic. First, it assumes that simple cells receive input that is scaled linearly by changes in contrast, e.g., the input has contrast-invariant orientation tuning; it then argues that addition of divisive or "normalizing" inhibition will explain response nonlinearities without disturbing input tuning for spatial properties such as orientation. We have instead emphasized that both the LGN input and the circuit are nonlinear, e.g., key nonlinearities in LGN responses are the c-d growth of the mean, saturation of the F1, and advance of the response phase. Second, the normalization model's explanations of temporal nonlinearities require unrealistically high membrane time constants. The model proposes that the phase advance and the high-temporal-frequency cutoff F at a given contrast are determined by the membrane time constant τ. c-d nonlinearities are explained by decreases in τ with increasing contrast, induced by the increase in membrane conductance from the normalizing inhibition. However, V1 cells often show low-contrast [or even high-contrast (Saul and Humphrey 1992)] cutoff (frequency showing little or no response) at $F = 10$–15 Hz (Albrecht 1995; Carandini et al. 1997, Fig. 7). For such a cutoff to be simply due to τ, one must have $\tau > 1/F$, i.e., greater than 66–100 ms (see footnote 2). Yet time constants of cortical cells in vivo are only 15–24 ms (Hirsch et al. 1998) at rest, and can only decrease under visual stimulation. Similarly, a 20° c-d phase shift in response to a 2-Hz stimulus (a temporal advance of 28 ms) would require a c-d decrease in τ of 28 ms.[3] Such a large decrease between 10 and 80% contrast seems unlikely.

The normalization model also requires divisive inhibition that depends only on contrast, independent of orientation. This is necessary, for example, to explain contrast saturation or c-d phase shifts of responses to nonpreferred stimuli. Experimental data now show that there is a contrast-dependent conductance increase that, at preferred orientations, can be as high as two- or threefold, but which is tuned for orientation (Anderson et al. 2000; Borg-Graham et al. 1998; Hirsch et al. 1998). The corresponding reduction in time constant can certainly *contribute* to phase advance (Fig. 8, "no A, no D") and to the threshold effect that we argue explains contrast-dependent changes in temporal frequency tuning. However, any such contribution will have orientation tuning like that of the conductances. Another significant problem is that the normalization model assumes that shunting inhibition will give this divisive effect, whereas recent theoretical studies suggest that the effect will be subtractive rather than divisive (Holt and Koch 1997).

Another model (that of Chance et al. 1998) independently arrived at some of the same qualitative ideas that we have developed here (see Chance et al. 1997; Priebe et al. 1997). In particular, they also pointed out that synaptic depression of feed-forward synapses could contribute to c-d phase advance, although they found $<4°$ of c-d shift per 3 octaves of contrast at 2 Hz (their Fig. 2*E*) and, curiously, did not find any c-d shift for temporal frequencies of 8 Hz or higher. They did not address the other nonlinear response properties or mechanisms

[3] For $2\pi f\tau \ll 1$, e.g. $f \ll 8$ Hz for typical cortical resting time constants in vivo of $\tau = 20$ ms (Hirsch et al. 1998), $\arctan(2\pi f\tau)/2\pi f \approx \tau$, hence the phase advance (footnote 1) simply becomes $\tau_0 - \tau_1$.

addressed here and did not address the coexistence of linear-like and nonlinear response properties.

Conclusion: origins of nonlinear and linear response properties

As the circuit model presented here has emphasized, many aspects of cortical processing are inherently nonlinear, including spike thresholds, adaptation, synaptic depression, conductance effects, and the contrast dependence of the input. On the other hand, many spiking responses of cat simple cells can be understood roughly in terms of linear filtering of the stimulus (e.g., DeAngelis et al. 1995; Sclar and Freeman 1982; Skottun et al. 1987, 1991a). Based on these findings, one theoretical approach is to consider simple cells as a rectified linear filter, and to seek nonlinear corrections that can give a more complete account of spiking responses (e.g., Albrecht and Geisler 1991; Carandini et al. 1997, 1998).

While this approach is useful in describing spiking behavior, we suggest that when mechanistic explanations are sought, the problem should be turned on its head. Simple cell responses must be understood in terms of cortical cells and circuits, which are inherently nonlinear. The greatest difficulty is explaining why the behavior of the cortical circuit appears linear in key respects. For example, understanding how orientation tuning comes to be contrast invariant has been a key problem for understanding V1 circuitry (Ben-Yishai et al. 1995; Somers et al. 1995; Troyer et al. 1998). As we have seen here, the particulars of the circuitry that achieve this linear-like behavior for orientation tuning need not generalize to other response properties, such as temporal frequency tuning. Thus we suggest that the key mechanistic question is not why simple-cell properties are nonlinear, but rather how they come to appear linear. Once the latter has been explained in a circuit model, one can see to what extent other, nonlinear behavior may emerge naturally from such biological nonlinearities as thresholds, synaptic depression, adaptation, and conductance changes.

APPENDIX A: DETAILS OF COMPUTATIONAL METHODS

Here we present the full details of the methods necessary to replicate our work.

Elements in common to both rate and spiking models

ARCHITECTURE. Both rate and spiking models are structured as follows. There are geniculocortical (G) synaptic weights connecting the LGN to the cortex, and two types of intracortical weights, excitatory-to-excitatory (E) and inhibitory-to-excitatory (I) (Fig. 1). The intracortical connections instantiate the cat layer 4 circuit model proposed in Troyer et al. (1998).

GENICULATE RESPONSES. Geniculate firing rates in response to drifting sinusoidal stimuli are modeled, as in Troyer et al. (1998), as linear rate modulations (rectified at 0 Hz) about background rates of 15 and 10 Hz for ON and OFF cells, respectively. ON cell modulations were at the stimulus phase, and OFF cell modulations lagged by 180°. Prerectification modulation amplitudes were chosen for each contrast and temporal frequency so that the first harmonic (F1) of the rectified rate modulations matched data from Sclar (1987, Fig. 1),[4] except in "flat" simulations, in which these amplitudes were set to four arbitrary values (15, 30, 60, and 90 Hz) that were held constant across temporal frequencies. To assign contrast values C to the flat amplitudes, we used matlab's "curvefit" function to fit the prerectification F1 values R at each temporal frequency for ON cells (matched to the Sclar data) with Naka-Rushton curves (Albrecht 1995)

$$R(C) = R_{\max} C^n/(C^n + C_{50}^n) \quad (A1)$$

From the fit curves we found the corresponding contrasts for each prerectification F1 at each temporal frequency. We then combined the data derived from flat inputs with those from Sclar inputs to generate contrast saturation curves (Fig. 4). Experimental contrast-saturation data were also fit to Naka-Rushton curves using curvefit.

The prerectification F1s as chosen above were further modified by use of the center-surround LGN spatial filter (Linsenmeier et al. 1982; Peichl and Wassle 1979) as in Troyer et al. (1998). All gratings were shown at the preferred spatial frequency of the model cortical cells [0.635°/cycle (Troyer et al. 1998)], so the prerectification modulation amplitude was reduced by the amount predicted by this filter relative to its value at the preferred spatial frequency of the LGN cell spatial filter (0.54 cycle/deg).

CORTICAL RFS. The distribution of LGN synaptic weights to a simple cell was described by a Gabor function (Jones and Palmer 1987), as in Troyer et al. (1998), "default" parameters.

SYNAPTIC DEPRESSION. The equations used to model synaptic depression are described in APPENDIX B. We examined synaptic depression in each of the three types of weights (G, E, and I) in the rate model, but only in the G weights in the spiking model. In both models, weight values must be changed when depression parameters are changed [to maintain the network in a stable range, Troyer et al. (1998, Fig. 13)]. Exploration of such parameter dependence is computationally expensive in the spiking model, so we did not explore intracortical depression in that model.

Rate model

In the rate model, the LGN was structured as a 31×31, $6.8° \times 6.8°$ retinotopic grid of cells, with retinotopic position varying linearly across the grid. ON cells were positioned at the vertices of the grid, while OFF cells lay at the center of each square within the grid; this offset is motivated by Wassle et al. (1981). The choice of a 31×31 grid in the rate model, versus 30×30 grid in the spiking model, was made simply so that a single ON cell would lie at the center of the grid.

We examined 192 model cortical simple cells (96 excitatory and 96 inhibitory) located at the single retinotopic position defined by the central LGN ON neuron. Each set of 96 cells represented each combination of 12 evenly spaced orientations (at 8–173°, to minimize grid discretization error) and 8 evenly spaced spatial phases (0–315°). Responses were studied to gratings of optimal spatial frequency and with orientation 38° (again chosen to minimize discretization effects). Responses for a given parameter set are the average over responses of all eight excitatory cells preferring 38°.

In the rate model, geniculocortical weights were set to the value of the Gabor at the corresponding retinal position, where positive (negative) values of the Gabor correspond to weights from ON (OFF) inputs. Connections between cortical cells were correlation-based, as in

[4] Throughout, we normalize the F1 to equal the amplitude of the sinusoidal component at the frequency of the grating stimulus. If the LGN input has temporal frequency ω, this normalized F1 is given by the sum of the amplitudes of the ω and $-\omega$ frequency components of the Fourier transform, when that transform is normalized so that the F0 or DC is the mean rate; this normalization is standard in neurophysiology (Skottun et al. 1991b). We have previously (Troyer et al. 1998) incorrectly stated that this normalization of the F1 requires that the Fourier transform have an extra factor of two relative to the normalization that makes the F0 equal to the mean rate. This mistake was due to our neglect of the $-\omega$ component, which has equal amplitude to the ω component; the factor of two is accounted for by including the negative as well as positive frequency components.

Troyer et al. (1998) with $n_{pow} = 5$, except that there was no stochasticity: connection strengths were simply set equal to the connectivity function $C(a, b)$ defined in that reference.

Dynamically, neurons in the rate model obeyed the following equations. Let $r_k^{I/E}(t)$ = the firing rate of inhibitory/excitatory cell k at time t, $v_k^{I/E}(t)$ = the voltage of inhibitory/excitatory cell k at time t, $\tau_m^{I/E}$ = the time constant of the inhibitory/excitatory cell membrane, $G_k(t)$ = the geniculocortical input to cell k at time t, $w_{kj}^{e \leftarrow i/e}(t)$ = the synaptic efficacy of the connection from inhibitory/excitatory cell j to excitatory cell k at time t, $\theta^{I/E}$ = the firing threshold for inhibitory/excitatory cells, and *floor* = a floor on the membrane voltage of the cells (see below). The firing rate for excitatory or inhibitory cell k is

$$r_k^E(t) = [v_k^E(t) - \theta^E]^+$$

$$r_k^I(t) = [v_k^I(t) - \theta^I]^+$$

where $[x]^+ = x$, $x > 0$; $= 0$, otherwise. The activity update for inhibitory cell k is

$$\tau_m^I \frac{dv_k^I}{dt} = -v_k^I(t) + G_k(t)$$

The inputs to excitatory cell k from geniculocortical, inhibitory, and intracortical excitatory sources are

$$n_k(t) = G_k(t) - \sum_{j=1}^{N} w_{kj}^{e \leftarrow i}(t) r_j^I(t) + \sum_{j=1}^{N} w_{kj}^{e \leftarrow e}(t) r_j^E(t)$$

where N is the number of excitatory or inhibitory neurons. The activity update for the excitatory cell k is

$$\tau_m^E \frac{dv_k^E}{dt} = -v_k^E(t) + n_k(t), \quad v_k^E > floor \tag{A2}$$

$$= [-v_k^E(t) + n_k(t)]^+, \quad v_k^E = floor \tag{A3}$$

Outside of the (fixed) f and τ values for depression, the rate model had eight parameters: the membrane time constants, the firing thresholds, and the gains of G, I, and E weights, as well as the voltage floor. The gains were scalars representing the summed synaptic strength of each type (G, I, E) received by each cell. This normalization was achieved by multiplicatively scaling all weights of a given type on a given cell. The voltage floor was the value below which any neuron's membrane potential was not allowed to go; if the membrane potential attempted to drop below the floor, it was clamped to the floor potential. This was included merely to represent the lower bound on the membrane voltage imposed in real neurons by the potassium reversal potential. This floor was somewhat arbitrarily set to -30, but this value was not critical; the behavior of the model was quantitatively similar for a floor value of -75, and only marginally different for a very "depolarized" floor value of -5.

Outputs of the model (excitatory cells only) were determined and averaged across the appropriate cells. The seven parameters other than the floor were then determined by searches through this seven-parameter space for all parameter combinations that satisfied the following criteria:

1) $\tau_m^E > \tau_m^I$ (McCormick et al. 1985).

2) $\theta^E > \theta^I$ (McCormick et al. 1985).

3) Standard deviation of the orientation tuning curve $<0.20°$ at all contrasts (defined as $\sqrt{\Sigma_i r_i(\theta_i - \theta_0)^2/\Sigma_i r_i}$, where r_i is the response to the ith orientation θ_i, and θ_0 is the preferred orientation of the cell studied).

4) Invariance of orientation tuning width with contrast (Sclar and Freeman 1982), defined as a ratio of the standard deviation of a Gaussian fit to the orientation tuning curve at low (10%) and high (80%) contrast between 4:5 and 5:4.

5) "Amplification ratio" >1 and <5 for both 10 and 80% contrast preferred orientation sinusoidal gratings (defined as ratio of F1 of voltage response with full cortical circuitry intact to F1 of voltage response induced by geniculocortical inputs alone); these values are comparable to the limits suggested in Ferster et al. (1996) for responses to 2 Hz, 64% contrast drifting sinusoidal gratings at the preferred orientation.

6) Mean cortical firing rates between 10 and 30 Hz for preferred orientation stimulus at 80% contrast.

Parameter searches were performed separately for each temporal frequency of stimulation. In Fig. 7, we show all parameter sets that satisfied these criteria at a given temporal frequency, without regard for whether the criteria were also satisfied at other temporal frequencies. All other figures show only those parameter sets that satisfied the criteria across all temporal frequencies, except that requirements on F1 ratios and mean cortical firing rates at high contrast were not enforced for temporal frequencies >8 Hz or for the flat F1 value of 15 Hz (these exceptions were made because responses at these frequencies and for these inputs were too small to meet the criteria). For the "no depression" case, the low bound on mean firing rate at high contrast was also relaxed slightly (to >9.5 Hz) to allow generation of a contrast saturation curve (Fig. 4).

The range of values of the seven parameters over which we conducted our search was as follows. For four of these parameters, this range varied with the location(s) of depressing synapses; for example, the relative strength of inhibition required to prevent cortical runaway was much less when intracortical excitatory depression (E depression) was present. For cases in which E depression was present, we searched through all combinations of the following values for these four parameters:

1) $\theta^E = 2, 4, 6$

2) G gain $= 1.0, 2.0, 4.0, 8.0$

3) $I \rightarrow E$ gain $= 0.15, 0.25, 0.35, 0.45$

4) $E \rightarrow E$ gain $= 0.06, 0.09, 0.12, 0.15$

When E depression was absent, we instead searched through all combinations of the following values for these four parameters:

1) $\theta^E = 3, 6, 9$

2) G gain $= 0.5, 1.0, 2.0, 4.0$

3) $I \rightarrow E$ gain $= 0.25, 0.35, 0.45, 0.55$

4) $E \rightarrow E$ gain $= 0.02, 0.04, 0.06, 0.08$

In all cases, we searched through all combinations of the following values for the remaining three parameters:

5) $\tau_m^E = 8, 12, 16$ ms

6) $\tau_m^I = \tau_m^E/2$

7) $\theta^I = 1, 2, 3$, with $\theta^I < \theta^E$

The number of combinations searched was 1,344 when E depression was present, 1,536 when it was absent. Note that we biased our selection toward smaller membrane time constants than those reported in vitro (20 ms for excitatory, 12 ms for inhibitory neurons) (McCormick et al. 1985), and in vivo in the absence of a stimulus (15–24 ms for excitatory cells) (Hirsch et al. 1998), to account for the additional conductances opened during stimulation.

The c-d phase advance was found by subtracting the phase of the F1 of the cortical response to 10% contrast gratings from that to 80% contrast gratings. As most simulations were of 2 s duration, phase analysis was performed on the last 500 ms, when the geniculocortical and intracortical excitatory depressing synapses would have reached steady state. [Intracortical inhibitory synapses fit to the train data ($\tau =$ 1,017 ms) would not have reached steady state, but the influence of the inhibitory depression is weak. We found in several example cases that examining the last second of 6-s runs caused negligible changes in results.]

The activity and depression equations were discretized using simple first-order Euler methods and 2-ms bins. Test runs using 0.25-ms resolution demonstrated that this bin size caused negligible changes in our results.

Spiking model

The spiking model was implemented as in Troyer et al. (1998). All parameters were as in that reference except for the overall synaptic strengths of geniculocortical and intracortical synapses. These values were determined, after sampling the synaptic weights as just described, by multiplying all synaptic weights of a given type (G, E, or I) by a single constant to set the total strength of such synapses. These values were chosen to constrain the standard deviation of the orientation tuning curve to be $<0.20°$ at all contrasts, as in the rate model, and to ensure contrast invariance at all temporal frequencies. Synaptic strength is defined in terms of the integrated current response induced when the cell is voltage clamped at V_{thresh} and all synapses of a given type are activated once (Troyer et al. 1998). Each excitatory cell received a total inhibitory synaptic strength of -14.726 nA ms, and a total intracortical excitatory synaptic strength of 3.112 nA ms, yielding mean unitary conductance values of $\bar{g}_{\text{in}} = 7.59$ nS and $\bar{g}_{\text{ex}}^{\text{ctx}} = 0.37$ nS. We used three separate values for the total geniculocortical synaptic strength onto each cortical cell, depending on the parameters used for geniculocortical depression: "no depression," 3.112 nA ms, with mean unitary conductance $\bar{g}_{\text{ex}}^{\text{gc}} = 0.32$; "pulse" parameters, 8.86 nA ms, with a mean unitary conductance of $\bar{g}_{\text{ex}}^{\text{gc}} = 0.92$ nS; "train" parameters, 26.45 nA ms, with a mean unitary conductance of $\bar{g}_{\text{ex}}^{\text{gc}} = 2.7$ nS. Note that we held total inhibition fixed, although we could have reduced this value when depression was present [because depression attenuates the untuned (DC) component of the geniculocortical input]. Since total inhibition is a free parameter, and reducing (increasing) inhibition broadens (tightens) both orientation and temporal frequency tuning, we have some freedom to control these tuning widths, yet remain within the experimental constraints.

The results presented here for the spiking model show model responses to drifting gratings at 105°. After a 500-ms "blank stimulus," during which time the cortical and LGN cells fired at background rates, a moving grating stimulus was presented for one second. Phase advances were calculated by first constructing a histogram of responses from 10 repetitions of the same stimulus condition, and then taking the Fourier transform of the final 500 ms of these histograms. We compared the difference in the phase of the response to 80 and 10% contrast gratings on a cell-by-cell basis, for all excitatory neurons with preferred orientation in the 5°-wide bin around 105° (preferred orientations 102.5 through 107.4°); there were 29 such excitatory neurons for the orientation map used.

APPENDIX B: A RATE MODEL OF SYNAPTIC DEPRESSION

We model synaptic depression as in Abbott et al. (1997; see also Tsodyks and Markram 1997): following a spike, the synaptic efficacy is multiplied by the fraction f, where $0 \leq f \leq 1$, and between spikes the efficacy recovers with time constant τ toward its undepressed value. It is clear how to model this in a spiking model, but not in a rate model. To determine this, we first derive an equation that behaves appropriately for the spiking model, and then derive a rate model equation as an appropriate average of this spiking model equation.

We begin with the spiking model equation. Let $w(t)$ be the efficacy at time t. Let the presynaptic spike train be denoted by $\rho(t) = \Sigma_i \delta(t - t_i)$, where presynaptic spike times are denoted as t_i and $\delta(x)$ is the Dirac delta function. Our desired equation is of the form

$$\tau \frac{\mathrm{d}w}{\mathrm{d}t} = -w(t) + w_{\max} - \tau c \rho(t) w(t) \tag{B1}$$

where c is a to-be-determined constant. In the absence of a presynaptic spike ($\rho = 0$), w decays exponentially toward $w_{\max}$ with time constant τ, as desired. The form of the last term is determined by the fact that the change in efficacy after a spike *1*) is proportional to the current value of the efficacy, $w(t)$; *2*) is proportional to $\rho(t)$ (so that it is zero in the absence of a spike, and infinite—an infinite value of $\mathrm{d}w/\mathrm{d}t$, and thus a discontinuous change in w—in the presence of a spike). In addition, *3*) the term must have the same dimensions as w, achieved by multiplying by τ, leaving c as a dimensionless constant.

The value of c is determined as follows. Let the times infinitesimally before and after t_i be denoted t_i^- and t_i^+, respectively. Depression is represented by the equation $w(t_i^+) = fw(t_i^-)$. To determine the spike-induced change in w, we integrate *Eq. B1* from t_i^- to t_i^+; because this is an infinitesimal interval, only integrands that are infinite during that interval give a nonzero result. Because w changes discontinuously, $\mathrm{d}w/\mathrm{d}t$ is infinite in the interval; so too is the term involving $\rho(t)$. The other two terms integrate to zero and can be neglected. However, we cannot simply integrate $\tau[cp(t)w(t)]$, because we do not know how $w(t)$ itself is changing over the interval—e.g., should $w(t)$ be $w(t_i^+)$ or $w(t_i^-)$? To solve this, we divide *Eq. B1* by $w(t)$ and multiply by $\mathrm{d}t/\tau$ before integrating, yielding[5]

$$\int_{w(t_i^-)}^{w(t_i^+)} \frac{\mathrm{d}w}{w} = -c \int_{t_i^-}^{t_i^+} \sum_j \delta(t - t_j)\mathrm{d}t \tag{B2}$$

or

$$c = -\ln \frac{w(t_i^+)}{w(t_i^-)} = -\ln f \tag{B3}$$

Thus our equation for synaptic depression is

$$\tau \frac{\mathrm{d}w}{\mathrm{d}t} = -w(t) + w_{\max} + \tau(\ln f)\rho(t)w(t) \tag{B4}$$

which can be integrated to yield

$$w(t) = w(0) \exp\left[-\frac{t}{\tau} + N(t, 0) \ln f \right] + \frac{w_{\max}}{\tau} \int_0^t \mathrm{d}t_1 \exp\left[-\frac{(t - t_1)}{\tau} + N(t, t_1) \ln f \right] \tag{B5}$$

where $N(t_2, t_1) \equiv \int_{t_1}^{t_2} \rho(s)ds$ is the spike count in the interval (t_1, t_2).

We now derive an equation for the mean efficacy, $\bar{w}(t) = E[w(t)]$, in terms of the mean rate, $r(t) = E[\rho(t)]$. Here $E[\cdot]$ means an expectation over a set of stochastic realizations. We assume the spike train $\rho(t)$ is a Poisson process with mean rate $r(t)$, so the expectation value is over Poisson realizations of spike trains. The spike count, $N(t_2, t_1)$, is Poisson distributed with mean $\int_{t_1}^{t_2} r(s)ds$. The equation for $\bar{w}(t)$ is found by taking the expectation value of both sides of *Eq. B5*, where nonstochastic quantities can be brought outside the expectation values

$$\bar{w}(t) = w(0) \exp\left(-\frac{t}{\tau} \right) E\{\exp[N(t, 0) \ln f]\} + \frac{w_{\max}}{\tau} \int_0^t \mathrm{d}t_1 \exp\left[-\frac{(t - t_1)}{\tau} \right] E\{\exp[N(t, t_1) \ln f]\} \tag{B6}$$

Thus to compute $\bar{w}(t)$, we must compute expectation values of the

[5] Note that these operations yield a term, $\frac{1}{\tau} \int_{t_i}^{t_i^+} \frac{w_{\max}}{w(t)} \mathrm{d}t$, which could also in principle be nonzero, if $w(t) = 0$. However, $w(t)$ can never reach zero for nonzero f and finite τ.

form $E[\exp(c\eta)]$, where η is Poisson-distributed with mean m

$$E[\exp(c\eta)] = \sum_{k=0}^{\infty} P(\eta = k)\exp(ck) = \sum_{k=0}^{\infty} \exp(-m)\left(\frac{m^k}{k!}\right)\exp(ck) \tag{B7}$$

$$= \exp(-m)\sum_{k=0}^{\infty}\frac{[m\exp(c)]^k}{k!} = \exp(-m)\exp[m\exp(c)] \tag{B8}$$

$$= \exp[-m(1-e^c)] \tag{B9}$$

Applying this result to *Eq. B6* yields

$$\bar{w}(t) = w(0)\exp\left[-\frac{t}{\tau} - (1-f)\bar{N}(t,0)\right] + \frac{w_{\max}}{\tau}\int_0^t dt_1 \exp\left[-\frac{(t-t_1)}{\tau} - (1-f)\bar{N}(t,t_1)\right] \tag{B10}$$

where $\bar{N}(t_2, t_1)$ is the mean number of spikes resulting between times t_1 and t_2 from a Poisson process with mean rate $r(t)$.

Finally, the differential equation for $d\bar{w}(t)/dt$ that produces *Eq. B10* as a solution is

$$\tau\frac{d\bar{w}}{dt} = -\bar{w}(t) + w_{\max} - \tau(1-f)r(t)\bar{w}(t) \tag{B11}$$

where we have noted that the mean rate $r(t) = E[\rho(t)]$ is given by $r(t) = d\bar{N}(t, 0)/dt$. Note that for $f = 1$ (i.e., no depression), the depression term disappears, as it should. This equation (discretized, i.e., $d\bar{w}/dt$ replaced by $\Delta w/\Delta t$) serves as the update rule in the rate model.

We thank A. Krukowski, T. Troyer, and A. Hoffman for many useful conversations and assistance with simulations, B. Bialek for outlining to us what is now in APPENDIX B, and S. Lisberger for reading a preliminary draft of the manuscript.

This work was supported by a Biomedical Engineering Research Grant from the Whitaker Foundation, a Searle Scholar's Award, an Alfred P. Sloan Foundation Research Fellowship, and National Eye Institute Grant RO1-EY-11001, all to K. D. Miller.

REFERENCES

ABBOTT LF, VARELA JA, SEN K, AND NELSON SB. Synaptic depression and cortical gain control. *Science* 275: 220–224, 1997.

ALBRECHT DG. Visual cortex neurons in monkey and cat: effect of contrast on the spatial and temporal phase transfer functions. *Vis Neurosci* 12: 1191–1210, 1995.

ALBRECHT DG, FARRAR SB, AND HAMILTON DB. Spatial contrast adaptation characteristics of neurones recorded in the cat's visual cortex. *J Physiol (Lond)* 347: 713–739, 1984.

ALBRECHT DG AND GEISLER WS. Motion selectivity and the contrast-response function of simple cells in the visual cortex. *Vis Neurosci* 7: 531–546, 1991.

ALLISON JD, MELZER P, DING Y, BONDS AB, AND CASAGRANDE V. Differential contributions of magnocellular and parvocellular pathways to the contrast response of neurons in bush baby primary visual cortex (V1). *Vis Neurosci* 17: 71–76, 2000.

ANDERSON JS, CARANDINI M, AND FERSTER D. Orientation tuning of input conductance, excitation, and inhibition in cat primary visual cortex. *J Neurophysiol* 84: 909–926, 2000.

BASKYS A. Metabotropic receptors and 'slow' excitatory actions of glutamate agonists in the hippocampus. *Trends Neurosci* 15: 92–96, 1992.

BEN-YISHAI R, BAR-OR RL, AND SOMPOLINSKY H. Theory of orientation tuning in visual cortex. *Proc Natl Acad Sci USA* 92: 3844–3848, 1995.

BLASDEL GG AND FITZPATRICK D. Physiological organization of layer 4 in macaque striate cortex. *J Neurosci* 4: 880–895, 1984.

BONDS AB. Temporal dynamics of contrast gain in single cells of the cat striate cortex. *Vis Neurosci* 6: 239–255, 1991.

BORG-GRAHAM LJ, MONIER C, AND FRÉGNAC Y. Visual input evokes transient and strong shunting inhibition in visual cortical neurons. *Nature* 393: 369–373, 1998.

BULLIER J AND HENRY GH. Laminar distribution of first-order neurons and afferent terminals in cat striate cortex. *J Neurophysiol* 42: 1271–1281, 1979.

CARANDINI M AND HEEGER DJ. Summation and division by neurons in visual cortex. *Science* 264: 1333–1336, 1994.

CARANDINI M, HEEGER DJ, AND MOVSHON JA. Linearity and normalization in simple cells of the macaque primary visual cortex. *J Neurosci* 17: 8621–8644, 1997.

CARANDINI M, HEEGER DJ, AND MOVSHON JA. Linearity and gain control in V1 simple cells. In: *Cerebral Cortex*, edited by Jones EG and Peters A. New York: Plenum, 1998, vol. 13.

CHANCE FS, NELSON SB, AND ABBOTT LF. Effects of synaptic depression of temporal nonlinearities in responses of model simple cells. *Soc Neurosci Abstr* 23: 1266, 1997.

CHANCE FS, NELSON SB, AND ABBOTT LF. Synaptic depression and the temporal response characteristics of V1 cells. *J Neurosci* 18: 4785–4799, 1998.

CHENG H, CHINO YM, SMITH EL, HAMAMOTO J, AND YOSHIDA K. Transfer characteristics of lateral geniculate nucleus X neurons in the cat: effects of spatial frequency and contrast. *J Neurophysiol* 74: 2548–2557, 1995.

CHINO YM, CHENG H, SMITH EL 3RD, GARRAGHTY PE, ROE AW, AND SUR M. Early discordant binocular vision disrupts signal transfer in the lateral geniculate nucleus. *Proc Natl Acad Sci USA* 91: 6938–6942, 1994.

CHUNG S AND FERSTER D. Strength and orientation tuning of the thalamic input to simple cells revealed by electrically evoked cortical suppression. *Neuron* 20: 1177–1189, 1998.

DEAN AF AND TOLHURST DJ. Factors influencing the temporal phase of response to bar and grating stimuli for simple cells in the cat striate cortex. *Exp Brain Res* 62: 143–151, 1986.

DEANGELIS GC, OHZAWA I, AND FREEMAN RD. Spatiotemporal organization of simple-cell receptive fields in the cat's striate cortex. II. Linearity of temporal and spatial summation. *J Neurophysiol* 69: 1118–1135, 1993.

DEANGELIS GC, OHZAWA I, AND FREEMAN RD. Receptive-field dynamics in the central visual pathways. *Trends Neurosci* 18: 451–458, 1995.

FERSTER D. Orientation selectivity of synaptic potentials in neurons of cat primary visual cortex. *J Neurosci* 6: 1284–1301, 1986.

FERSTER D. Spatially opponent excitation and inhibition in simple cells of the cat visual cortex. *J Neurosci* 8: 1172–1180, 1988.

FERSTER D. X- and Y-mediated current sources in areas 17 and 18 of cat visual cortex. *Vis Neurosci* 4: 135–145, 1990a.

FERSTER D. X- and Y-mediated synaptic potentials in neurons of areas 17 and 18 of cat visual cortex. *Vis Neurosci* 4: 115–133, 1990b.

FERSTER D, CHUNG S, AND WHEAT H. Orientation selectivity of thalamic input to simple cells of cat visual cortex. *Nature* 380: 249–252, 1996.

FERSTER D AND JAGADEESH B. Nonlinearity of spatial summation in simple cells of areas 17 and 18 of cat visual cortex. *J Neurophysiol* 66: 1667–1679, 1991.

GEISLER WS AND ALBRECHT DG. Cortical neurons: isolation of contrast gain control. *Vision Res* 32: 1409–1410, 1992.

GIL Z, CONNORS BW, AND AMITAI Y. Differential regulation of neocortical synapses by neuromodulators and activity. *Neuron* 19: 679–686, 1997.

GILBERT CD. Laminar differences in receptive field properties of cells in cat primary visual cortex. *J Physiol (Lond)* 268: 391–421, 1977.

HAWKEN MJ AND PARKER AJ. Contrast sensitivity and orientation selectivity in lamina IV of the striate cortex of old world monkeys. *Exp Brain Res* 54: 367–372, 1984.

HAWKEN MJ, SHAPLEY RM, AND GROSOF DH. Temporal frequency tuning of neurons in macaque V1: effects of luminance contrast and chromaticity. *Invest Ophthalmol Vis Sci Suppl* 33: 955, 1992.

HEEGER DJ. Normalization of cell responses in cat striate cortex. *Vis Neurosci* 9: 181–198, 1992.

HIRSCH JA, ALONSO J-M, REID RC, AND MARTINEZ LM. Synaptic integration in striate cortical simple cells. *J Neurosci* 18: 9517–9528, 1998.

HOLT GR AND KOCH C. Shunting inhibition does not have a divisive effect on firing rates. *Neural Comput* 9: 1001–1013, 1997.

HOLUB RA AND MORTON-GIBSON M. Response of visual cortical neurons of the cat to moving sinusoidal gratings: response-contrast functions and spatiotemporal interactions. *J Neurophysiol* 46: 1244–1259, 1981.

HUBEL DH AND WIESEL TN. Receptive fields, binocular interaction and functional architecture in the cat's visual cortex. *J Physiol (Lond)* 160: 106–154, 1962.

JONES JP AND PALMER LA. An evaluation of the two-dimensional Gabor filter model of simple receptive fields in cat striate cortex. *J Neurophysiol* 58: 1233–1258, 1987.

KAPLAN E, PURPURA K, AND SHAPLEY RM. Contrast affects the transmission of visual information through the mammalian lateral geniculate nucleus. *J Physiol (Lond)* 391: 267–288, 1987.

KRUKOWSKI AE. *A Model of Cat Primary Visual Cortex and Its Thalamic Input* (PhD thesis). San Francisco, CA: University of California, 2000.

KRUKOWSKI AE AND MILLER KD. Thalamocortical NMDA conductances and intracortical inhibition can explain cortical low-pass temporal tuning. *Nature Neurosci* 4: 424–430, 2001.

LARKUM ME, ZHU JJ, AND SAKMANN B. A new cellular mechanism for coupling inputs arriving at different cortical layers. *Nature* 398: 338–341, 1999.

LINSENMEIER RA, FRISHMAN LJ, JAKIELA HG, AND ENROTH-CUGELL C. Receptive field properties of X and Y cells in the cat retina derived from contrast sensitivity measurements. *Vision Res* 22: 1173–1183, 1982.

MARKRAM H AND TSODYKS M. Redistribution of synaptic efficacy between neocortical pyramidal neurons. *Nature* 382: 807–810, 1996.

MCCORMICK DA. Membrane properties and neurotransmitter actions. In: *The Synaptic Organization of the Brain*, edited by Shepard G. Oxford, UK: Oxford, 1990, p. 32–66.

MCCORMICK DA, CONNORS BW, LIGHTHALL JW, AND PRINCE DA. Comparative electrophysiology of pyramidal and sparsely spiny stellate neurons of the neocortex. *J Neurophysiol* 54: 782–805, 1985.

NELSON S, TOTH L, SHETH B, AND SUR M. Orientation selectivity of cortical neurons during intracellular blockade of inhibition. *Science* 265: 774–777, 1994.

NELSON SB. Temporal interactions in the cat visual system. I. Orientation-selective suppression in the visual cortex. *J Neurosci* 11: 344–356, 1991a.

NELSON SB. Temporal interactions in the cat visual system. III. Pharmacological studies of cortical suppression suggest a presynaptic mechanism. *J Neurosci* 11: 369–380, 1991b.

NICOLL RA. The coupling of neurotransmitter receptors to ion channels in the brain. *Science* 241: 545–551, 1988.

OHZAWA I, SCLAR G, AND FREEMAN RD. Contrast gain control in the cat's visual system. *J Neurophysiol* 54: 651–667, 1985.

PEICHL L AND WASSLE H. Size, scatter and coverage of ganglion cell receptive field centres in the cat retina. *J Physiol (Lond)* 291: 117–141, 1979.

PRIEBE NJ, KAYSER AS, KRUKOWSKI AE, AND MILLER KD. A model of simple cell orientation tuning: the role of synaptic depression. *Soc Neurosci Abstr* 23: 2061, 1997.

REICH DS, VICTOR JD, KNIGHT BW, OZAKI T, AND KAPLAN E. Response variability and timing precision of neuronal spike trains in vivo. *J Neurophysiol* 77: 2836–2841, 1997.

SANCHEZ-VIVES MV, MCCORMICK DA, AND NOWAK LG. Is synaptic depression prevalent in vivo and does it contribute to contrast adaptation. *Soc Neurosci Abstr* 24: 896, 1998.

SAUL AB AND HUMPHREY AL. Spatial and temporal response properties of lagged and nonlagged cells in cat lateral geniculate nucleus. *J Neurophysiol* 64: 206–224, 1990.

SAUL AB AND HUMPHREY AL. Evidence of input from lagged cells in the lateral geniculate nucleus to simple cells in cortical area 17 of the cat. *J Neurophysiol* 68: 1190–1208, 1992.

SCLAR G. Expression of "retinal" contrast gain control by neurons of the cat's lateral geniculate nucleus. *Exp Brain Res* 66: 589–596, 1987.

SCLAR G AND FREEMAN RD. Orientation selectivity in the cat's striate cortex is invariant with stimulus contrast. *Exp Brain Res* 46: 457–461, 1982.

SCLAR G, MAUNSELL JH, AND LENNIE P. Coding of image contrast in central visual pathways of the macaque monkey. *Vision Res* 30: 1–10, 1990.

SHAPLEY RM AND VICTOR JD. The effect of contrast on the transfer properties of cat retinal ganglion cells. *J Physiol (Lond)* 285: 275–298, 1978.

SKOTTUN BC, BRADLEY A, SCLAR G, OHZAWA I, AND FREEMAN RD. The effects of contrast on visual orientation and spatial frequency discrimination: a comparison of single cells and behavior. *J Neurophysiol* 57: 773–786, 1987.

SKOTTUN BC, DE VALOIS RL, GROSOF DH, MOVSHON JA, ALBRECHT DG, AND BONDS AB. Classifying simple and complex cells on the basis of response modulation. *Vision Res* 38: 1079–1086, 1991a.

SKOTTUN BC, GROSOF DH, AND DE VALOIS RL. On the responses of simple and complex cells to random dot patterns. *Vision Res* 31: 43–46, 1991b.

SOMERS D, NELSON SB, AND SUR M. An emergent model of orientation selectivity in cat visual cortical simple cells. *J Neurosci* 15: 5448–5465, 1995.

SONG S, VARELA JA, TURRIGIANO G, ABBOTT LF, AND NELSON SB. The dynamics of synaptic depression at monosynaptic inhibitory inputs to visual cortical pyramidal neurons. In: *Proceedings of the Computational Neuroscience Meeting, CNS98*, edited by Bower JM. New York: Plenum, 1999.

STRATFORD KJ, TARCZY-HORNOCH K, MARTIN KA, BANNISTER NJ, AND JACK JJ. Excitatory synaptic inputs to spiny stellate cells in cat visual cortex. *Nature* 382: 258–261, 1996.

TANG AC, BARTELS AM, AND SEJNOWSKI TJ. Effects of cholinergic modulation on responses of neocortical neurons to fluctuating input. *Cereb Cortex* 7: 502–509, 1997.

TARCZY-HORNOCH K. *Physiology of Synaptic Inputs to Layer IV of Cat Visual Cortex* (PhD thesis). Oxford, UK: Oxford University, 1996.

TARCZY-HORNOCH K, MARTIN KA, JACK JJ, AND STRATFORD KJ. Synaptic interactions between smooth and spiny neurons in layer 4 of cat visual cortex in vitro. *J Physiol (Lond)* 508: 351–363, 1998.

THOMSON AM, DEUCHARS J, AND WEST DC. Single axon excitatory postsynaptic potentials in neocortical interneurons exhibit pronounced paired pulse facilitation. *Neuroscience* 54: 347–360, 1993.

TROYER TW, KRUKOWSKI A, PRIEBE NJ, AND MILLER KD. Contrast-invariant orientation tuning in cat visual cortex: feedforward tuning and correlation-based intracortical connectivity. *J Neurosci* 18: 5908–5927, 1998.

TROYER TW AND MILLER KD. Integrate-and-fire neurons matched to physiological f-I curves yield high input sensitivity and wide dynamic range. In: *Computational Neuroscience*: *Trends in Research 1997*, edited by Bower JM. New York: Plenum, 1997a, p. 197–201.

TROYER TW AND MILLER KD. Physiological gain leads to high ISI variability in a simple model of a cortical regular spiking cell. *Neural Comput* 9: 971–983, 1997b.

TSODYKS MV AND MARKRAM H. The neural code between neocortical pyramidal neurons depends on neurotransmitter release probability. *Proc Natl Acad Sci USA* 94: 719–723, 1997.

WASSLE H, BOYCOTT BB, AND ILLING RB. Morphology and mosaic of on- and off-beta cells in the cat retina and some functional considerations. *Proc R Soc Lond B Biol Sci* 212: 177–195, 1981.